

Aus dem Institut für Tierschutz, Tierverhalten und Versuchstierkunde
des Fachbereichs Veterinärmedizin der Freien Universität Berlin

In Kooperation mit der
Klinik für Radiologie
Charité – Universitätsmedizin Berlin

**Entwicklung und Evaluierung neuer niedrig-molekularer
Sonden für die Charakterisierung von
Gefäßerkrankungen mittels der
Magnetresonanztomographie (MRT)**

**Inaugural-Dissertation
zur Erlangung des Grades eines
Doktors der Veterinärmedizin
an der
Freien Universität Berlin**

vorgelegt von
Carolin Reimann
Tierärztin aus Hagenow

Berlin 2020
Journal-Nr.: 4195

Aus dem Institut für Tierschutz, Tierverhalten und Versuchstierkunde
des Fachbereichs Veterinärmedizin der Freien Universität Berlin

In Kooperation mit der
Klinik für Radiologie
Charité – Universitätsmedizin Berlin

**Entwicklung und Evaluierung neuer niedrig-molekularer Sonden für die
Charakterisierung von Gefäßerkrankungen mittels der Magnetresonanztomographie (MRT)**

Inaugural-Dissertation
zur Erlangung des Grades eines
Doktors der Veterinärmedizin
an der
Freien Universität Berlin

vorgelegt von
Carolin Reimann
Tierärztin aus Hagenow

Berlin 2020
Journal-Nr.:4195

Gedruckt mit Genehmigung des Fachbereichs Veterinärmedizin
der Freien Universität Berlin

Dekan: Univ.-Prof. Dr. Jürgen Zentek
Erster Gutachter: Univ.-Prof. Dr. Christa Thöne-Reineke
Zweiter Gutachter: Prof. Dr. Marcus Richard Makowski
Dritter Gutachter: Univ.-Prof. Dr. Achim Gruber

*Deskriptoren (nach CAB-Thesaurus):
animal models; mice; atherosclerosis; inflammation; radiography; magnetic resonance imaging; contrast agents; histology; immunofluorescence*

Tag der Promotion: 28.07.2020

Bibliografische Information der *Deutschen Nationalbibliothek*
Die Deutsche Nationalbibliothek verzeichnet diese Publikation in der Deutschen Nationalbibliografie; detaillierte bibliografische Daten sind im Internet über <<https://dnb.de>> abrufbar.

ISBN: 978-3-96729-114-8

Zugl.: Berlin, Freie Univ., Diss., 2020

Dissertation, Freie Universität Berlin

D188

Dieses Werk ist urheberrechtlich geschützt.

Alle Rechte, auch die der Übersetzung, des Nachdruckes und der Vervielfältigung des Buches, oder Teilen daraus, vorbehalten. Kein Teil des Werkes darf ohne schriftliche Genehmigung des Verlages in irgendeiner Form reproduziert oder unter Verwendung elektronischer Systeme verarbeitet, vervielfältigt oder verbreitet werden.

Die Wiedergabe von Gebrauchsnamen, Warenbezeichnungen, usw. in diesem Werk berechtigt auch ohne besondere Kennzeichnung nicht zu der Annahme, dass solche Namen im Sinne der Warenzeichen- und Markenschutz-Gesetzgebung als frei zu betrachten wären und daher von jedermann benutzt werden dürfen.

This document is protected by copyright law.

No part of this document may be reproduced in any form by any means without prior written authorization of the publisher.

alle Rechte vorbehalten | all rights reserved

© Mensch und Buch Verlag 2021

Choriner Str. 85 - 10119 Berlin

verlag@menschundbuch.de – www.menschundbuch.de

Inhaltsverzeichnis

1. Einleitung	5
1.1 Atherosklerose.....	5
1.2 Atherosklerotischer Plaque	6
1.3 Extrazelluläre Matrix	7
1.4 Elastin.....	8
1.5 Matrixmetalloproteininasen.....	9
1.6 Molekulare Bildgebung mittels Magnetresonanztomographie	10
1.7 Tiermodell ApoE -/- Maus.....	12
2. Druckfassung der ausgewählten Publikationen	15
2.1 Contrast-enhanced magnetic resonance angiography using a novel elastin-specific molecular probe in an experimental animal model	15
2.2 Dual-probe molecular MRI for the <i>in vivo</i> characterization of atherosclerosis in a mouse model: <i>Simultaneous assessment of plaque inflammation and extracellular-matrix remodeling</i>	27
3. Diskussion.....	47
4. Zusammenfassung	51
5. Summary „Development and Evaluation of new low-molecular probes for the characterization of vascular diseases by magnetic resonance imaging (MRI)“	53
6. Literaturverzeichnis der Einleitung und Diskussion	55
7. Publikationsliste.....	59
8. Danksagung	61
9. Selbstständigkeitserklärung.....	63

1. Einleitung

1.1 Atherosklerose

Atherosklerose ist eine Krankheit, bei der sich das Innere einer Arterie aufgrund der Bildung von atherosklerotischen Plaques verengt [1]. Die Verengung geht mit einer Verhärtung und mit einem Elastizitätsverlust der betroffenen Arterie einher. Die Verengung der Arterien begrenzt den Fluss von sauerstoffreichem Blut zu anderen Körperteilen. Atherosklerose ist gekennzeichnet durch eine Umgestaltung der Arterien, die zu einer subendothelialen Anreicherung von Fettstoffen führt, welche Plaques genannt werden. Die Atherosklerose ist eine der häufigsten Ursachen für Morbidität und Mortalität in der westlichen Welt sowie in den Entwicklungsländern und gilt als einer der Hauptverursacher von Herz-Kreislauf-Erkrankungen [2]. Klinische Manifestationen von Atherosklerose, wie akuter Myokardinfarkt und Schlaganfall, sind weltweit nach wie vor die Hauptursachen für Tod und körperliche Beeinträchtigungen, obwohl sich in den letzten Jahren ein breites Bewusstsein für diese Krankheit entwickelt hat [3]. In den nächsten Jahrzehnten wird aufgrund der zunehmenden Alterung der westlichen Bevölkerung und einer erheblichen Zunahme der Risikofaktoren, einschließlich Übergewicht, Diabetes, Bluthochdruck und Hypercholesterinämie, auch eine erhebliche Zunahme der Inzidenz von Herz-Kreislauf-Erkrankungen erwartet [4, 5]. Die letzten Jahrzehnte der Forschung auf dem Gebiet der Atherosklerose haben neue molekulare Wege in der Entstehung von Atherosklerose (Atherogenese) und neue Mechanismen aufgezeigt, die zu Komplikationen bei humanen atherosklerotischen Plaques führen [1, 6-8]. Dieser Fortschritt in unserem Verständnis der Pathogenese der Atherosklerose hat neue Perspektiven für die Früherkennung, die Überwachung und die Behandlung eröffnet. Betreffen kann die Atherosklerose besonders die mittleren und großen Arterien des Herzens, des Gehirns, der Nieren, anderer lebenswichtiger Organe und der unteren Extremitäten. Für eine Vielzahl kardiovaskulärer Folgeerkrankungen ist Atherosklerose von fundamentaler Bedeutung. Mit dem Fortschreiten der Atherosklerose kommt es zu progredienten Stenosierungen der Gefäße sowie ggf. zu thromboembolischen Ereignissen. Die Atherosklerose ist durch die Ansammlung von Lipiden und fibrösem Gewebe in der Gefäßintima gekennzeichnet [9]. Atherosklerotische Plaques bestehen aus drei Hauptkomponenten: (1.) Zelluläre Komponente, einschließlich glatter Muskelzellen, Makrophagen und andere Leukozyten; (2.) Extrazelluläre Matrix (ECM), einschließlich Kollagen, Elastinfasern und Proteoglykane; sowie (3.) Intrazelluläre und extrazelluläre Lipide [9]. Die Entstehung von Atherosklerose ist ein komplexer Prozess, bei dem proinflammatorische Zellen dynamisch einströmen und die Plaque last progressiv zunimmt,

was mit einer Neusynthese von extrazellulären Matrixproteinen verbunden ist [10]. Eine Behandlung der Atherosklerose mit Statinen verhindert oder verringert die Einwanderung von Entzündungszellen und die Bildung von Matrix-Metalloproteasen (MMP). Durch das so vermehrt vorhandene Kollagen, das nicht durch MMP's abgebaut wird, wird die Plaque-Stabilität auf lange Sicht erhöht. Die Behandlung mit Statinen führt zur allgemeinen Senkung des Blutcholesterinspiegels und ist deshalb mit der Verbesserung der Endothelfunktion assoziiert. Die Statintherapie, als effektiv cholesterinsenkende und makrophagendeaktivierende Therapie, verringert also die kardiovaskuläre Ereignisrate und verzögert das Fortschreiten der Atherosklerose. Bezüglich der zeitlichen Entwicklung ist die Atherosklerose durch einen initial langsamen Krankheitsverlauf gekennzeichnet und bleibt in den meisten Fällen bis zum Endstadium der Erkrankung asymptomatisch. Plötzliche auftretende Oberflächenerosion oder Risse an der Plaqueoberfläche können in Gefäßverschlüssen resultieren, welche subsequent zu einem Myokardinfarkt oder Schlaganfall führen [11].

1.2 Atherosklerotischer Plaque

Ein früher Marker für Atherosklerose ist die endotheliale Dysfunktion. Bevor es zu strukturellen Veränderungen der Gefäßwand kommt, kommt es erst zu endothelialen Dysfunktionen wie erhöhte Endothelpermeabilität, Thrombozytenaggregation und Leukozytenadhäsion [12]. Der Schwerpunkt der Entwicklung atherosklerotischer Plaques liegt auf arteriellen Remodeling. Arterielles Remodeling beinhaltet Veränderungen in der Morphologie und der strukturellen Integrität der Gefäßwand, die insbesondere bei pathologischen Prozessen wie der Atherosklerose von Bedeutung ist. Die als Remodeling bezeichneten Umbauprozesse in der Gefäßwand führen zu einer Größenzunahme des Gefäßquerschnitts. Die pathologischen Veränderungen der Gefäßwand bei atherosklerotischen Erkrankungen treten hauptsächlich in der Tunica intima auf. Eine endotheliale Dysfunktion führt zu einem Einstrom von LDL mit Bildung von Fettstreifen und anschließend zur Entwicklung einer komplexen Läsion. Diese Läsionen sind durch die Migration und Proliferation glatter Muskelzellen, die Expression extrazellulärer Matrixproteine und die Bildung eines oder mehrerer lipidreicher Kerne gekennzeichnet. Ein dynamisches Gleichgewicht zwischen der ECM-Synthese durch hauptsächlich glatte Muskelzellen und dem Abbau durch MMPs steuert die verfügbare Menge und beeinflusst das Fortschreiten der atherosklerotischen Erkrankung. Die hauptsächlich in der ECM vorkommenden Proteine sind

verschiedenen Arten von Kollagen- und Elastinfasern, die mit Proteoglykanen und Glykosaminoglykanen durchsetzt sind. Wenn die den Lipidkern überdeckende faserige Kappe dünner wird, kann ein Plaquebruch, der zur Thrombusbildung und möglicherweise zum Gefäßverschluss führt, die klinische Folge sein [7]. In der folgenden Abbildung sind die Prozesse der Entwicklung eines atherosklerotischen Plaques schematisch dargestellt.

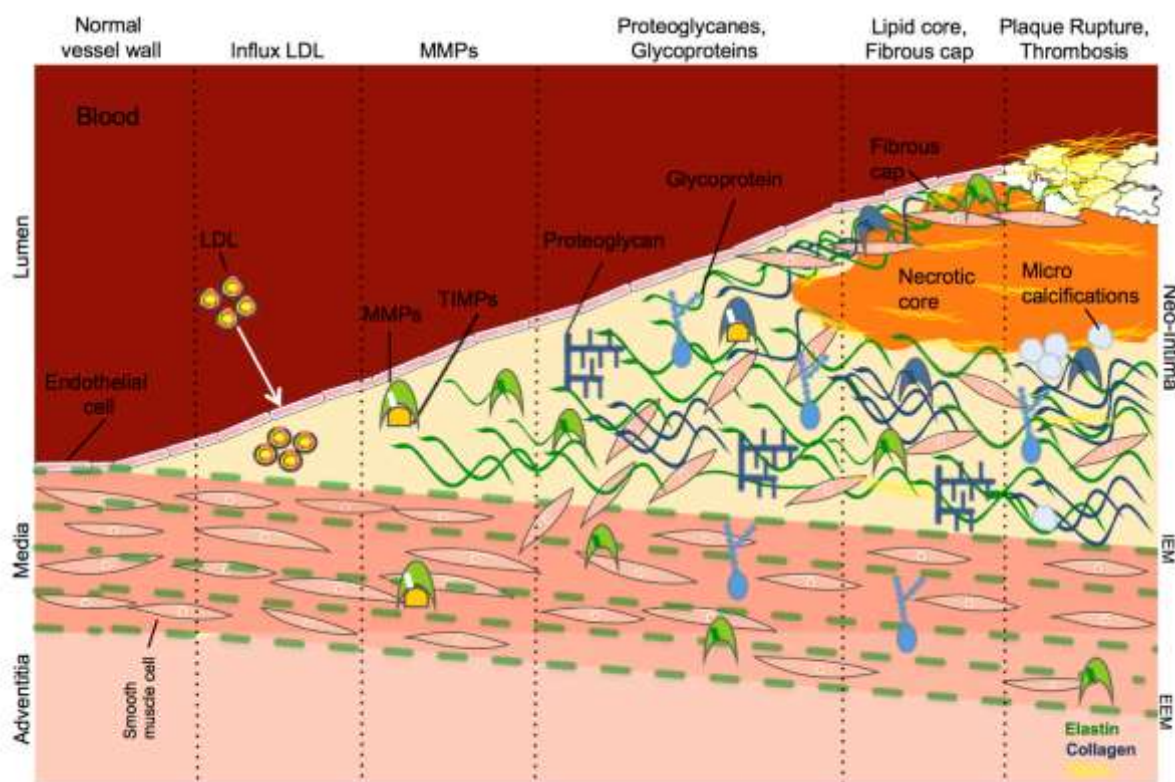


(Abbildung entnommen aus Reimann C, Brangsch J, Colletini F, Walter T, Hamm B, Botnar RM, Makowski MR. Molecular imaging of the extracellular matrix in the context of atherosclerosis. *Advanced drug delivery reviews*. 2017;113:49-60)

1.3 Extrazelluläre Matrix

Besondere Berücksichtigung bei atherosklerotischen Gefäßwanderkrankungen gilt der extrazellulären Matrix (ECM). Die ECM ist in biologischen Geweben allgegenwärtig und besteht hauptsächlich aus verschiedenen Arten von Kollagen- und Elastinfasern, die die am häufigsten vorkommenden extrazellulären Matrixproteine darstellen [13]. Die ECM ist der häufigste Bestandteil sowohl der normalen Gefäßwand als auch der atherosklerotischen Plaques, einschließlich der fibrösen Kappe, die dem atherosklerotischen Plaque aufliegt. Ein

dynamisches Gleichgewicht zwischen ECM-Synthese und Abbau kontrolliert die verfügbare Menge an ECM und beeinflusst das Fortschreiten der atherosklerotischen Erkrankung. In der Matrix von atherosklerotischen Plaques synthetisieren glatte Muskelzellen, Fibroblasten und in geringerem Maße Makrophagen ECM-Proteine und scheiden diese aus. Dieselben und weitere Zelltypen, einschließlich Endothelzellen, Makrophagen, glatte Muskelzellen, T-Lymphozyten und Mastzellen, sezernieren ECM-abbauende Enzyme. Hierzu zählen Metalloproteininasen, Cathepsine, Serinproteasen, Chymase und Tryptase [14]. Diese Enzyme zeigen eine starke proteolytische Aktivität, insbesondere bei anfälligen oder instabilen atherosklerotischen Läsionen [15, 16]. Infolgedessen werden extrazelluläre Matrixkomponenten fragmentiert und ihre Gesamtmenge wird verringert. Dies führt zu einer Ausdünnung der fibrösen Kappe. Daher kann der ECM-Abbau Plaqueregionen anfälliger für Störungen machen und Instabilität prädisponieren [17].

1.4 Elastin

Elastin ist das dominierende Protein der ECM und wird hauptsächlich in der Tunica Media der „gesunden“ Arterienwand abgelagert [18]. Es trägt bis zu 50% zum Trockengewicht der Arterien bei. In Venen wird es in niedrigeren Konzentrationen exprimiert. Elastin spielt eine wichtige strukturelle Rolle bei der Aufrechterhaltung der Integrität der Arterienwand. Es trägt erheblich zur Zugfestigkeit von großen und kleinen Arterien bei und ermöglicht die Aufrechterhaltung einer dauerhaften mechanischen Belastung durch arterielle Pulsation und intravaskulären Druck. Elastin wird von vaskulären glatten Muskelzellen synthetisiert. Die Produktion beginnt mit der Synthese und Sekretion des löslichen Vorläufers Tropoelastin [13]. Nach der posttranslationalen Modifikation wird Tropoelastin vernetzt und zu Elastinpolymeren organisiert, welche konzentrische Ringe aus elastischen Lamellen um das arterielle Lumen bilden. Der Grad der Elastinvernetzung hängt mit der Zugfestigkeit der extrazellulären Matrix und damit der arteriellen Gefäßwand zusammen [19]. Die Fülle an Elastin und seine erhöhte Expression während der Plaqueentwicklung machen dieses extrazelluläre Matrixprotein zu einem vielversprechenden bildgebenden Biomarker [20, 21]. Verschiedene histopathologische Studien haben dazu gezeigt, dass Elastin während der Entstehung von Atherosklerose ein wichtiger Bestandteil der extrazellulären Matrix ist [13, 18, 22]. Aufgrund seines hohen Vorkommens ist es besonders nützlich als Biomarker für die Magnetresonanztomographie (MRT) und ermöglicht die Bildgebung mit einer hohen räumlichen Auflösung. Eine hohe räumliche Auflösung ist wichtig für die Visualisierung

morphologischer und biologischer Veränderungen in der dünnen arteriosklerotischen Arterienwand. Neben seiner strukturellen Rolle hat Elastin wichtige biologische Signal- und Regulationsfunktionen während der arteriellen Entwicklung und zur Kontrolle der Proliferation von z.B. proinflammatorischen Zellen in der Gefäßwand [23]. Mehrere pathologische Reize sind für die Auslösung der Elastogenese bei Atherosklerose verantwortlich, einschließlich der Proliferation von glatten Muskelzellen [24, 25]. Dies führt zu einer deutlichen Erhöhung des Elastingehaltes während der Entwicklung atherosklerotischer Plaques [13, 18, 26]. Die relative ECM-Zusammensetzung des atherosklerotischen Plaques ist für das Fortschreiten des Plaques und die Unterscheidung zwischen stabilen und instabilen / anfälligen Plaques von hoher Relevanz. Neben der erhöhten Expression von Elastin während des Fortschreitens der atherosklerotischen Plaques führen verschiedene Faktoren zu einem Abbau und einer Fragmentierung von Elastin. Elastische Fasern werden gezielt von verschiedenen Matrix-Metalloproteininasen (MMPs), insbesondere von den Subtypen MMP 2 und MMP 9, angegriffen und abgebaut [27]. MMPs liegen unter normalen physiologischen Bedingungen bereits in latenter Form vor und werden nach einer Gefäßwandverletzung aktiviert [28, 29]. Elastolyse wird auch durch entzündliche Prozesse induziert. Die Verringerung der Elastizität der Tunica media ist ein Ergebnis einer verringerten Elastinexpression, einer Änderung der Elastinvernetzung und einer Elastolyse. Diese Prozesse erhöhen die Möglichkeit einer Gefäßschädigung und stellen daher einen potenziellen prädispositionellen Faktor für die Entstehung von Atherosklerose dar [30, 31]. Die bildliche Darstellung quantitativer Veränderungen von intraplaque Elastin liefert wichtige Informationen für die Beurteilung der Plaquezusammensetzung, insbesondere da vermutet wurde, dass humane atherosklerotische Plaques basierend auf ihrer relativen elastischen Faserzusammensetzung in stabile und instabile / anfällige Plaque-Typen unterschieden werden können [13].

1.5 Matrixmetalloproteininasen

Matrixmetalloproteininasen sind ECM-abbauende Proteininasen, die in den verschiedenen Entwicklungsstadien der Atherosklerose eine wichtige Rolle spielen [27]. Sie können von fast allen Zellen in der Plaque-Matrix sekretiert werden, einschließlich Makrophagen, Endothelzellen und glatten Muskelzellen [32]. Die meisten Zellen in der Plaque-Matrix haben Rezeptoren für strukturelle ECM-Komponenten. Daher wirken sich MMP indirekt auf die Zellfunktionen aus [33]. Die verschiedenen MMP-Subtypen können die Aufteilung

verschiedener Komponenten des ECM bewirken. Einige MMP-Subtypen sind pro-atherogen (MMP 2, 9), andere anti-atherogen (MMP 1, 3), und es wurde vermutet, dass einige keinen relevanten Einfluss auf die Entwicklung atherosklerotischer Plaques haben (MMP 7, 12, 13) [34]. Jedes MMP hat spezifische Zielsubstrate wie z.B. Kollagenase [35]. Eine unkontrollierte Zunahme der Aktivität von MMPs wurde mit dem Umbau der Matrix in Verbindung gebracht, welcher zu Gewebeschäden und funktionellen Veränderungen führt [36]. Es wurde gezeigt, dass MMPs eine entscheidende Rolle bei der Verdünnung und Schwächung der Plaque-Kappe spielen [29]. Verschiedene Studien haben hierzu gezeigt, dass die erhöhte Expression von insbesondere MMP 2 und MMP 9 eine wichtige Rolle bei der Ausdünnung der Faserkappe und der Destabilisierung von Plaques spielt [27, 37].

1.6 Molekulare Bildgebung mittels Magnetresonanztomographie

Im klinischen Alltag werden in erster Linie traditionelle Angiographietechniken verwendet, um den Grad der Lumenverengung in den Arterien zu bestimmen [38]. Obwohl angiographische Techniken der diagnostische Referenzstandard sind, verbessern nicht alle interventionellen Therapien die Prognose und das Outcome des Patienten [39]. Verschiedene Studien haben gezeigt, dass die höchste Anzahl an rupturierten atherosklerotischen Plaques in Arterien mit <60% der Stenose gefunden wurde [40]. Aktuell wird vermutet, dass der Stenosegrad und das Rupturrisiko von atherosklerotischen Plaques nicht immer direkt miteinander zusammenhängen [41]. Es wurde jedoch eine Reihe von Plaque-Merkmalen identifiziert, die mit einer erhöhten Ruptur-Wahrscheinlichkeit verbunden sind. Hierzu gehören der Influx entzündungsfördernder Zellen, das positive Gefäßwand-Remodeling, die Angiogenese, ein großer nekrotischer Kern, eine dünne fibrotische Kappe, Mikrokalzifikationen und Hämorragien innerhalb des Plaques. Um diese Veränderungen besser detektieren zu können, wurden verschiedene Methoden der invasiven und nichtinvasiven Bildgebung untersucht. Entzündungsaktivität und Plaquelastr, die beide durch molekulare MRT-Techniken sichtbar gemacht werden können, sind Schlüsselmerkmale gefährdeter atherosklerotischer Plaques. Die Erkennung und die Klassifizierung von Atherosklerose werden derzeit mittels molekularer Bildgebung erforscht. Bei der molekularen Magnetresonanztomographie (MRT) der Atherosklerose ist die Biologie der Atherosklerose und die Visualisierung geeigneter Zielstrukturen von besonderer Bedeutung. Das übergeordnete Ziel hierbei ist die Detektion von Ruptur gefährdeten Plaques, bevor es zu Folgen wie einem Myokardinfarkt oder einem Schlaganfall kommt. Aus pathophysiologischer

Sicht ist der Übergang von einem stabilen zu einem instabilen oder rupturgefährdeten atherosklerotischen Plaque die Folge komplexer Wechselwirkungen zwischen verschiedenen molekularen Bestandteilen des Plaques. Die molekulare Bildgebung ist ein neuartiger Ansatz zur nichtinvasiven Identifizierung dieser pathologischen Prozesse bei der Atherosklerose auf molekularer Ebene. Sie ermöglicht die direkte *in vivo*-Visualisierung biologischer Prozesse und versucht, die dynamischen Wechselwirkungen zwischen biologischen Komponenten während des Fortschreitens der Erkrankung durch Anwendung verschiedener Bildgebungstechniken in Kombination mit molekularen Sonden zu verstehen [42-44]. Im Gegensatz zu herkömmlichen klinischen Bildgebungsverfahren, wie Röntgenangiographie, zielt die molekulare Bildgebung darauf ab, molekulare Pathomechanismen sichtbar zu machen und zu quantifizieren, anstatt auf sich ergebende anatomische Veränderungen, z.B. Grad der Stenose [45, 46] zu fokussieren. Die Magnetresonanztomographie kann eine entscheidende Rolle in diesem speziellen Bereich der molekularen Bildgebung spielen. Sie ermöglicht die nichtinvasive Charakterisierung der relativen Plaque-Zusammensetzung, die Integrität der Faserkappe [99] und die Visualisierung der Gefäßwand, einschließlich der Quantifizierung der Plaque-Belastung. Dies kann durch multiparametrische Bildgebungsprotokolle in Kombination mit MR-Sonden erreicht werden, um einen Kontrast zwischen Plaque-Strukturen wie der Faserkappe und dem nekrotischen Kern zu erzeugen [47, 48]. Die meisten MRT-Sonden, insbesondere klinisch zugelassene Sonden, stammen von paramagnetischen Komplexen, einschließlich paramagnetischen Substanzen auf Gadolinium- (Gd-) Basis oder Eisenoxid-Nanopartikeln [49-51]. Basierend auf den jüngsten Entwicklungen in der molekularen und zellulären Bildgebungsorschung wurden auch andere Arten molekularer Bildgebungssonden entwickelt [52-54]. Sonden auf Gadoliniumbasis, insbesondere Sonden mit kleinem Molekulargewicht, die im klinischen Umfeld verwendet werden, bestehen aus einem chelatierten Gadolinium in Kombination mit einer zielspezifischen Stelle. Molekulare MRI-Nanopartikel bestehen in den meisten Fällen aus drei Teilen: (1) Nanopartikelkern zur Kontrastverstärkung; (2) wasserdispergierbare Hüllen zur Verhinderung einer unspezifischen Bindung sowie zur Erhöhung der Biokompatibilität und (3) bioaktive Materialien zur Zielerkennung und stabilisierten Beschichtung (z. B. Dextran) [55]. Magnetische Nanopartikel auf Eisenoxidbasis sind in variablen Größen erhältlich und bieten eine Reihe einzigartiger Eigenschaften für die molekulare Bildgebung [56]. Gd-basierte Sonden erzeugen durch die Verkürzung der T1-Relaxationszeit einen hellen oder positiven Kontrasteffekt [57]. Auf Eisenoxid basierende Nanopartikel liefern aufgrund der Verkürzung der T2 / T2 * -Relaxationszeit einen starken Dunkel-Negativ-Kontrast-Effekt [58]. Die Vorteile der MRT im Vergleich zu anderen bildgebenden Verfahren,

wie der Positron Emission Tomographie (PET) und der Einzelphotonen-Emissions-Computertomographie (SPECT) liegen darin, dass sie strahlungsfrei ist und die Bildgebung daher ohne damit verbundenen Risiken mehrmals wiederholt werden kann. Dies ist besonders im klinischen Umfeld relevant, da häufig Nachuntersuchungen erforderlich sind. Darüber hinaus ermöglicht die MRT die Detektion und Visualisierung von molekularen Sonden mit einer hohen räumlichen und zeitlichen Auflösung. Im Gegensatz zu PET, die eine zusätzliche Bildgebungseinheit zur anatomischen Lokalisierung der Sonde erfordert, ermöglicht die MRT auch die Erzeugung anatomischer Bilder, einschließlich der nativen Charakterisierung atherosklerotischer Plaque-Komponenten [59].

1.7 Tiermodell ApoE -/- Maus

Das Apolipoprotein-E-defiziente (ApoE -/-) Modell wurde 1992 durch homologe Rekombination embryonaler Stammzellen entwickelt und ist derzeit das am weitesten verbreitete präklinische Modell der Atherosklerose [60, 61]. Dieses Tiermodell ist für die Untersuchung der menschlichen Artherosklerose gut etabliert. Apolipoprotein-E ist ein Ligand für die Lipoproteinrezeptoren, der an der Erkennung und Aufnahme von Lipoproteinen aus dem Blut beteiligt ist. Atheroskleroseanfällige ApoE -/- Mäuse zeigen eine schlechte Lipoprotein Aufnahme mit anschließender Akkumulation von mit Cholesterinester angereicherten Partikeln im Blut. Durch das Fehlen des Apolipoprotein-E's entwickeln die ApoE -/- Mäuse folglich Hyperlipoproteinämie [62], schwere Hypercholesterinämie und atherosklerotische Läsionen. Arterielle Fettdepots können bereits 3 Monate nach der Geburt beobachtet werden [63, 64]. Die Entwicklung von Läsionen wird durch die Fütterung der westlichen Diät beschleunigt [65]. Mit zunehmendem Alter oder längerer Fütterungszeit der atherogenen westlichen Ernährung mit 21% Fett und 0.15% Cholesterol können an vielen Stellen in großen und mittleren Arterien Läsionen beobachtet werden. Die Läsionen in den ApoE -/- Mäusen sind durch Gefäßentzündungen [66] gekennzeichnet, die mit der Infiltration von Makrophagen und anderen Immunzellen verbunden sind [66]. Dieser systemische proinflammatorische Status von ApoE -/- Mäusen macht sie zudem zu einem guten Modell für die Untersuchung von Gefäßentzündungen. Es gibt aber nicht nur Vorteile in diesem Tiermodell. Zu den Limitationen zählen die Unterschiede zu humanen atherosklerotischen Plaques. Hier ist vor allem die Seltenheit von Plaqueabschwemmungen sowie Thrombose zu nennen [67]. Trotz kleiner Einschränkungen hat sich die ApoE -/- Maus aufgrund ihrer schnellen Reproduktion, einfachen genetischen Manipulation und der Fähigkeit, die Atherogenese in einem angemessenen Zeitrahmen auszubilden, als das vorherrschende Modell zur Untersuchung experimenteller Atherosklerose erwiesen.

Ziel des ersten Teils dieser Dissertation ist es, in einem translationalen Ansatz im Mausmodell eine neuartige elastinspezifische molekulare Sonde auf Gadoliniumbasis zu evaluieren und mit dem klinischen Kontrastmittel Gadobutrol für die Durchführung einer MR-Angiographie zu vergleichen. Im zweiten Teil der Dissertation wurden zwei verschiedenen molekulare Biomarker, eine elastinspezifische Sonde auf Gadoliniumbasis und einer makrophagenspezifische Sonde auf Eisenoxidbasis, simultan *in vivo* eingesetzt. Es wurde die Durchführbarkeit einer molekularen Multisonden-MRT zur simultanen Charakterisierung des strukturellen Umbaus der extrazellulären Matrix und der entzündlichen Aktivität für progressive Atherosklerose untersucht. Zu überprüfen galt, die Fähigkeit und Eignung der elastinspezifischen Sonde rupturgefährdete Plaques frühzeitig zu detektieren und zu charakterisieren sowie deren Ansprechen auf medikamentöse Therapien zu quantifizieren.

2. Druckfassung der ausgewählten Publikationen

2.1 Contrast-enhanced magnetic resonance angiography using a novel elastin-specific molecular probe in an experimental animal model

Autoren: Carolin Reimann, Julia Brangsch, Jan Ole Kaufmann, Lisa C. Adams, David C Onthank, Simon P Robinson, Rene M. Botnar, Federico Collettini, Marcus R. Makowski

Jahr: 2018

Journal: Contrast Media & Molecular Imaging

Published: 2018; Oct. 23. doi: 10.1155/2018/9217456

Bibliografische Quelle: Reimann C, Brangsch J, Kaufmann JO, Adams LC, Onthank DC, Robinson SP, Botnar RM, Collettini F, Makowski MR. Contrast-enhanced magnetic resonance angiography using a novel elastin-specific molecular probe in an experimental animal model. Contrast media & molecular imaging. 2018;2018:9217456

Hindawi
 Contrast Media & Molecular Imaging
 Volume 2018, Article ID 9217456, 9 pages
<https://doi.org/10.1155/2018/9217456>



Research Article

Contrast-Enhanced Magnetic Resonance Angiography Using a Novel Elastin-Specific Molecular Probe in an Experimental Animal Model

Carolin Reimann^{1,2}, Julia Brangsch^{1,2}, Jan Ole Kaufmann,¹ Lisa C. Adams,¹ David C. Onthank,³ Simon P. Robinson,³ Rene M. Botnar,^{4,5,6,7} Federico Collettini,¹ and Marcus R. Makowski^{1,4,5}

¹Charité–Universitätsmedizin Berlin, Corporate Member of Freie Universität Berlin, Humboldt-Universität zu Berlin, and Berlin Institute of Health, Charitéplatz 1, 10117 Berlin, Germany

²Department of Veterinary Medicine, Institute of Animal Welfare, Animal Behavior and Laboratory Animal Science, Freie Universität Berlin, Königsweg 67, Building 21, 14163 Berlin, Germany

³Lantheus Medical Imaging, North Billerica, MA, USA

⁴King's College London, School of Biomedical Engineering and Imaging Sciences United Kingdom, St Thomas' Hospital, Westminster Bridge Road, London SE1 7EH, UK

⁵BHF Centre of Excellence, King's College London, United Kingdom, Denmark Hill Campus, 125 Coldharbour Lane, London SE5 9NU, UK

⁶Wellcome Trust and EPSRC Medical Engineering Center, King's College London, Gibbs Building, 215 Euston Road, London NW1 2BE, UK

⁷Escuela de Ingeniería, Pontificia Universidad Católica de Chile, Santiago, Chile

Correspondence should be addressed to Carolin Reimann; carolin.reimann@charite.de

Received 16 January 2018; Revised 15 June 2018; Accepted 17 July 2018; Published 23 October 2018

Academic Editor: Luc Zimmer

Copyright © 2018 Carolin Reimann et al. This is an open access article distributed under the Creative Commons Attribution License, which permits unrestricted use, distribution, and reproduction in any medium, provided the original work is properly cited.

Objectives. The aim of this study was to test the potential of a new elastin-specific molecular agent for the performance of contrast-enhanced first-pass and 3D magnetic resonance angiography (MRA), compared to a clinically used extravascular contrast agent (gadobutrol) and based on clinical MR sequences. **Materials and Methods.** Eight C57BL/6J mice (BL6, male, aged 10 weeks) underwent a contrast-enhanced first-pass and 3D MR angiography (MRA) of the aorta and its main branches. All examinations were on a clinical 3 Tesla MR system (Siemens Healthcare, Erlangen, Germany). The clinical dose of 0.1 mmol/kg was administered in both probes. First, a time-resolved MRA (TWIST) was acquired during the first-pass to assess the arrival and washout of the contrast agent bolus. Subsequently, a high-resolution 3D MRA sequence (3D TI FLASH) was acquired. Signal-to-noise ratios (SNRs) and contrast-to-noise ratios (CNRs) were calculated for all sequences. **Results.** The elastin-specific MR probe and the extravascular imaging agent (gadobutrol) enable high-quality MR angiograms in all animals. During the first-pass, the probes demonstrated a comparable peak enhancement (300.6 ± 32.9 vs. 288.5 ± 33.1 , $p > 0.05$). Following the bolus phase, both agents showed a comparable intravascular enhancement (SNR: 106.7 ± 11 vs. 102.3 ± 5.3 ; CNR 64.5 ± 7.4 vs. 61.1 ± 7.2 , $p > 0.05$). Both agents resulted in a high image quality with no statistical difference ($p > 0.05$). **Conclusion.** The novel elastin-specific molecular probe enables the performance of first-pass and late 3D MR angiography with an intravascular contrast enhancement and image quality comparable to a clinically used extravascular contrast agent.

2. Druckfassung der ausgewählten Publikationen

Contrast Media & Molecular Imaging

1. Introduction

Contrast-enhanced magnetic resonance angiography (CE-MRA) has become the clinical reference technique for the evaluation of vascular territories and of associated pathologies in patients [1, 2]. CE-MRA angiography is performed, e.g., for the visualization of the aorta, the carotid arteries, the renal arteries, and most other arterial territories [1, 3]. Therefore, different techniques are currently in clinical use, including the first-pass angiography technique, which is usually performed in a single breath-hold. For this technique, the timing of the arterial bolus is of high importance to achieve the maximum arterial enhancement. Additionally, in most imaging protocols different phases are acquired, including the arterial, venous, and portal venous phase, depending on the clinical question [2]. The main advantage of this approach is the imaging of the different vascular phases with a high intravascular enhancement, whereas the main drawback is that due to the short scan time, only relatively large vascular structures can be visualized. A typical clinically used sequence type is the TWIST (time-resolved angiography with interleaved stochastic trajectories) sequence, which improves the temporal resolution of the sequence based on specific stochastic trajectories [4]. In clinical practice, an additional high-resolution 3D angiography (e.g., 3D T1 FLASH) is usually acquired at a relatively late time point with high spatial resolution. This type of sequence enables the visualization of relatively small vascular structures.

Recently, a novel small-molecular-weight gadolinium-based elastin-specific molecular agent has been introduced [5–8]. This probe has been used for different molecular applications, including the characterization of the arterial vascular wall in different vascular diseases, e.g., atherosclerosis, aortic aneurysms, or Marfan's disease [5–8]. Since this agent contains only a small targeting moiety in addition to a single gadolinium complex, this probe is comparable to currently clinically used contrast agents. To take full clinical advantage of the elastin agent, it would be preferable to also be able to gather the early blood phase clinical applications, including magnetic resonance angiographies (MRA).

The aim of this study was to test the potential of a small-molecular-weight gadolinium-based elastin-specific magnetic resonance (MR) probe for the performance of contrast-enhanced first-pass and late 3D MRA using clinical MR protocols in comparison to a clinically used extravascular contrast agent (gadobutrol).

2. Materials and Methods

2.1. Animal Experiments. All procedures were performed according to the guidelines and regulations of the Federation of Laboratory Animal Science Associations (FELASA) and the local guidelines and provisions for the implementation of the Animal Welfare Act. For imaging, eight ten-week-old male homozygous C57BL/6J mice from Charles River Laboratories (Edinburgh, United Kingdom) were used. All animals were housed in a clean barrier and fed with

a standard lab diet. Prior to the imaging sessions, mice were anesthetized using an intraperitoneal administration of a combination of medetomidine ($500\text{ }\mu\text{g/kg}$), fentanyl ($50\text{ }\mu\text{g/kg}$), and midazolam (5 mg/kg). Following the final imaging session, mice were euthanized. For histological examinations, a perfusion at a pressure of 100 mm Hg with the fixative MorFFFix® (Morphisto, Frankfurt am Main, Germany) was performed followed by excision of the carotid arteries, brachiocephalic artery, and aorta including the renal arteries. All animal procedures in this study were conducted by a veterinarian and all possible steps were taken to avoid animal suffering at each stage of the experiment.

2.2. Animal Handling and In Vivo Magnetic Resonance Imaging. The imaging sessions were performed using a clinical 3T Siemens system (Biograph, Siemens Healthcare, Erlangen, Germany) and a clinical single-loop coil (diameter 4 cm , Siemens Healthcare, Erlangen, Germany). During the imaging sessions, body temperature (37°C) was monitored using a MR-compatible heating system (Model 1025, SA Instruments Inc, Stony Brook, NY). For the administration of the different MR imaging agents, a small diameter tube with an attached needle was inserted into the tail vein of the animals. Following the acquisition of unenhanced scans, the administration of the imaging agents was performed.

2.3. Imaging Agents. As a “control” agent, gadobutrol (Gadovist®, Bayer Pharma AG, Berlin, Germany) was administered undiluted at a clinical dose of 0.1 mmol/kg bodyweight and followed by 0.01 ml saline. In a previous study, the R_1 relaxivity of gadobutrol at 3T was reported to be 3.6 ± 0.2 [9]. The elastin-specific molecular agent (ESMA, Lantheus Medical Imaging, North Billerica, Massachusetts, USA) was administered diluted to the same volume and at the same dose of 0.1 mmol/kg bodyweight. The unbound longitudinal relaxivity of the probe at 3T was reported to be 4.7 ± 0.1 [5]. The imaging agents were administered in a random order in the same animal. To allow for a complete clearance of the imaging agents, a seven-day time gap was left between both imaging sessions. Prior to the second imaging agent administration, an unenhanced scan (pre-scan) was performed in all imaging sessions in all animals to confirm that no residual agent remained in the vascular system.

2.4. Time-Resolved MR Angiography (TWIST) and High-Resolution 3D Angiography (FLASH). All imaging sequences used in this study were derived from a clinically used MR protocol and adapted for small animal imaging. For image acquisition the following sequence parameters were used. First, a low-resolution localizer scan was performed in sagittal, coronal, and transverse orientation to plan the subsequent imaging planes. The localizer scan had the following parameters: field of view 280 mm , matrix 256 , and slice thickness 6 mm . Subsequently, a TWIST (time-resolved angiography with interleaved stochastic trajectories) T1 angiography sequence was performed: Repetition

Contrast Media & Molecular Imaging

3

time (TR) 3.5 ms, echo time (TE) 1.3 ms 10 slices, flip angle 12°, 50 timepoints, field of view 316, matrix 480, interpolated inplane resolution 0.3 mm, and slice thickness 0.5 mm. For the late-phase high-resolution angiography, a 3D T1 FLASH (fast low angle shot) sequence was used: TR 4.7 ms, TE 1.9 ms, 60 slices, field of view 316, matrix 480, interpolated inplane resolution 0.3 mm, and slice thickness 0.5 mm.

2.5. Image Analysis of MR Angiograms. MR images were analyzed using OsiriX (version 7.1, OsiriX foundation). All images were analyzed in a random order and blinded to the imaging agent and the different time points. Signal-to-noise (SNR) and contrast-to-noise (CNR) measurements were performed in data sets of the time-resolved MR angiography (TWIST) and high-resolution 3D FLASH imaging. To quantify the vascular signal enhancement in the time-resolved TWIST sequence, signal measurements were performed using a region of interest in the left ventricle of the heart. To quantify the vascular signal enhancement in the T1 FLASH sequence, signal measurements were performed using a region of interest in the aortic lumen at the level of the heart. Noise measurements were performed anterior to the thorax with the standard deviation of the region of interest. The SNR was calculated as follows: $\text{SNR} = \text{mean signal (aortic lumen)} / \text{standard deviation signal (noise)}$. For the assessment of the contrast-to-noise ratio, an additional region of interest was placed in the muscle tissue dorsal of the aorta. The CNR was calculated as follows: $\text{CNR} = (\text{mean signal (aortic lumen)} - \text{mean signal (muscle tissue)}) / \text{standard deviation signal (noise)}$.

For the image quality assessment of the 3D T1 FLASH sequence, the image quality was ranked based on a five-point scale: 1 = poor quality information, 2 = aorta visible but markedly blood, 3 = aorta visible with moderate blurring, 4 = aorta visible with minimal blurring, and 5 = aorta visible with sharply defined borders. The image grading system used was modified based on the system by McConnell et al. [10].

2.6. Histological Analysis of Arterial Vessel System. The histological analysis was performed for the aorta, the brachiocephalic artery, and the carotid artery. The vessels were embedded in paraffin and cut into 5 μm thick serial sections. These sections were subsequently stained with Miller's Elastica van Gieson stain (EvG) and hematoxylin and eosin (HE).

2.7. Morphometry of the Arterial System. The complete arterial system including the carotid arteries, the subclavian arteries, brachiocephalic artery, aortic arch, and descending aorta to the iliac arteries was visualized in all MR scans. The vessel bifurcations, e.g., aorta to brachiocephalic artery, brachiocephalic artery to subclavian artery, were used as anatomical landmarks for coregistration of the *in vivo* MR images and *ex vivo* images from histology. The morphometrical analysis was performed using elastin-stained sections (Miller's Elastica van Gieson stain) and ImageJ software (Version 1.51f, ImageJ).

2.8. Statistical Analysis. Data are expressed as mean \pm standard deviation. To determine continuous variables Student's *t*-test (unpaired, 2-tailed) was used. Linear regression analysis and Bland-Altman analysis were used to compare the two contrast agents. For the first method, the slope of the regression line (*b*) together with the Pearson correlation coefficient (*R*) was calculated. For the latter method instead, the mean difference (*M*) with limits of agreement (*I*) (± 1.96 times the standard deviation) was calculated. $p < 0.05$ was used for significance.

3. Results

No side effects or adverse reactions to the imaging agents were observed in the investigated animals.

3.1. Time-Resolved First-Pass MR Angiography (TWIST). An example of the dynamic contrast enhancement using the elastin-specific molecular agent and gadobutrol is shown in Figures 1(a) and 1(b). The different signal-to-noise ratios (SNRs) and contrast-to-noise ratios (CNRs) derived from the time-resolved MR angiography (TWIST) for the evaluated probes are shown in Figures 2(a) and 2(b). A contrast enhancement curve, which is typical for extravascular contrast agents, was visualized. The elastin-specific molecular agent showed a slightly higher peak enhancement at approximately three seconds following the contrast injection, compared to the enhancement of gadobutrol (SNR: 300.6 ± 32.9 vs 288.5 ± 33.1 , $p > 0.05$; CNR: 65.3 ± 7.5 vs. 61.4 ± 7.7 , $p > 0.05$). For the peak enhancement, the average aortic SNR and CNR was not significantly different between the elastin-specific agent and the extracellular extravascular agent gadobutrol ($p > 0.05$). Also, in the later phases after more than 20 seconds, the average SNR and CNR between the contrast agents was not significantly different from each other ($p > 0.05$) for each time point measured.

3.2. High-Resolution 3D Angiography (T1 FLASH). A typical high-resolution 3D T1 FLASH angiography is shown in Figures 3(a) and 3(b). The SNRs and CNRs in the later bolus phase, approximately three minutes following the injection of the probes, demonstrated slightly higher values for the elastin-specific agent compared to the extracellular extravascular agent gadobutrol (Figure 4). The average SNR and CNR for the elastin-specific agent were 109.2 ± 16.6 and 65.4 ± 8.4 . The average SNR and CNR for the extracellular extravascular agent gadobutrol were 105.9 ± 10.4 and 61.1 ± 7.2 . No significant differences were measured between the two probes for the SNR ($p > 0.05$) and the CNR ($p > 0.05$).

3.3. Image Quality for the High-Resolution 3D FLASH Angiography. The image quality for both the elastin-specific molecular agent and the extracellular extravascular agent gadobutrol were high for the visualization of the thoracic and the abdominal aorta (Figure 5). For the elastin-specific agent and average image quality of 4.50

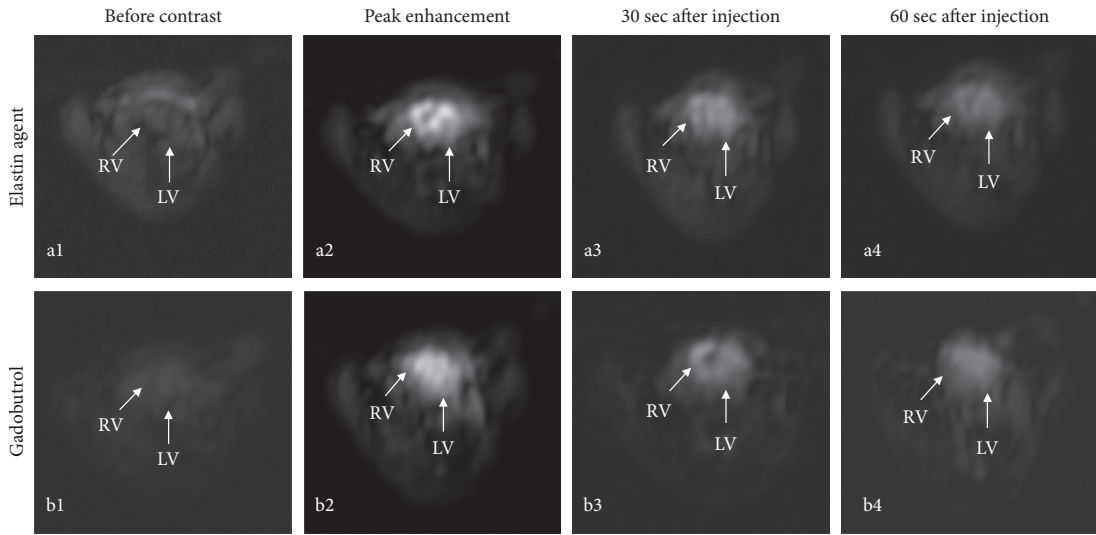


FIGURE 1: Example of a first-pass MR angiography (TWIST) following the administration of the elastin-specific molecular agent and the clinically used gadobutrol. (a, b) The images show the first-pass MR angiography (TWIST) following the administration of the elastin agent and the clinically used agent gadobutrol. (a1, b1) Precontrast images at the level of the heart show no relevant signal enhancement prior to the administration of the probes. (a2, b2) Immediately after the administration of the imaging agents, a high signal in the left and right ventricle can be appreciated during the first-pass. Visually, the signal intensity from both probes was comparable. (a3, b3) 30 seconds after the administration of the probes, a clear reduction of the signal at the level of the heart can be appreciated. (a4, b4) 60 seconds following the administration of the probes, a further decrease in signal can be appreciated. RV: right ventricle; LV: left ventricle.

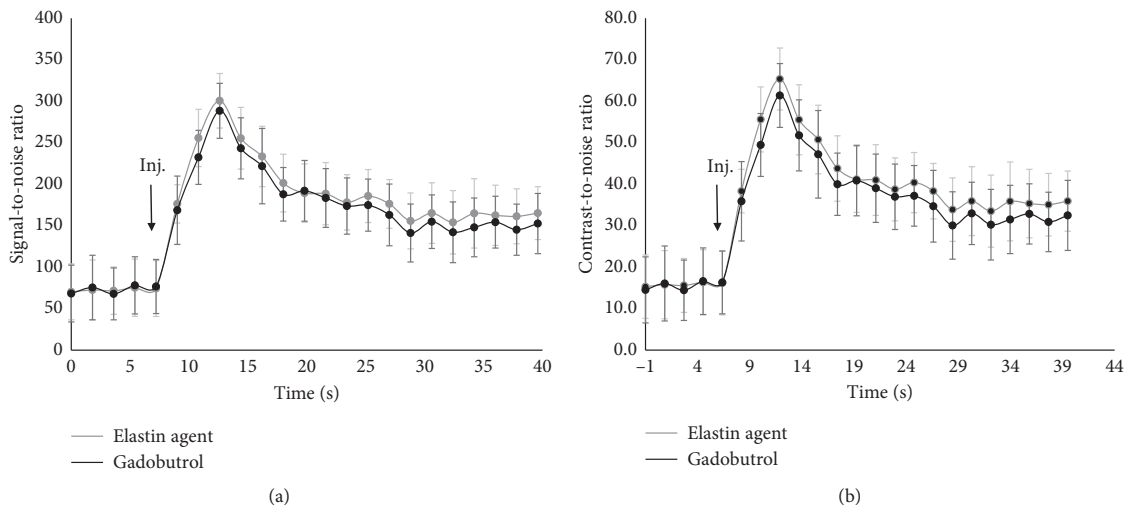


FIGURE 2: Signal-to-noise ratios and contrast-to-noise ratios in the first-pass MR angiography (TWIST) following the administration of the elastin-specific molecular agent and the clinically used agent gadobutrol. (a, b) Signal-to-noise and contrast-to-noise ratios of the first-pass and the early phases following the administration of the elastin-specific molecular agent and the clinically used gadobutrol ($n = 8$). A contrast enhancement curve, typical for extravascular imaging agents, was visualized. Signal-to-noise in contrast-to-noise measurements were performed in the left ventricle. Directly after administration, the peak enhancement was measured during the first-pass. The signal-to-noise in contrast-to-noise ratio derived from the elastin-specific agent was slightly, however not significantly ($p > 0.05$), higher compared to the enhancement derived from gadobutrol. This can be explained by the slightly higher relaxivity of the elastin-specific agent compared to gadobutrol. Following the first-pass, both agents show a comparable biokinetic of the reduction in signal. Inj.: injection of the respective probe.

± 0.53 and 4.38 ± 0.52 was measured for the aorta in the thorax and the abdomen. For the extravascular agent gadobutrol, an average image quality of 4.25 ± 0.71 and 4.13 ± 0.64

was measured for the aorta in the thorax and the abdomen. No significant difference was found between the two different imaging agents ($p \leq 0.05$).

Contrast Media & Molecular Imaging

5

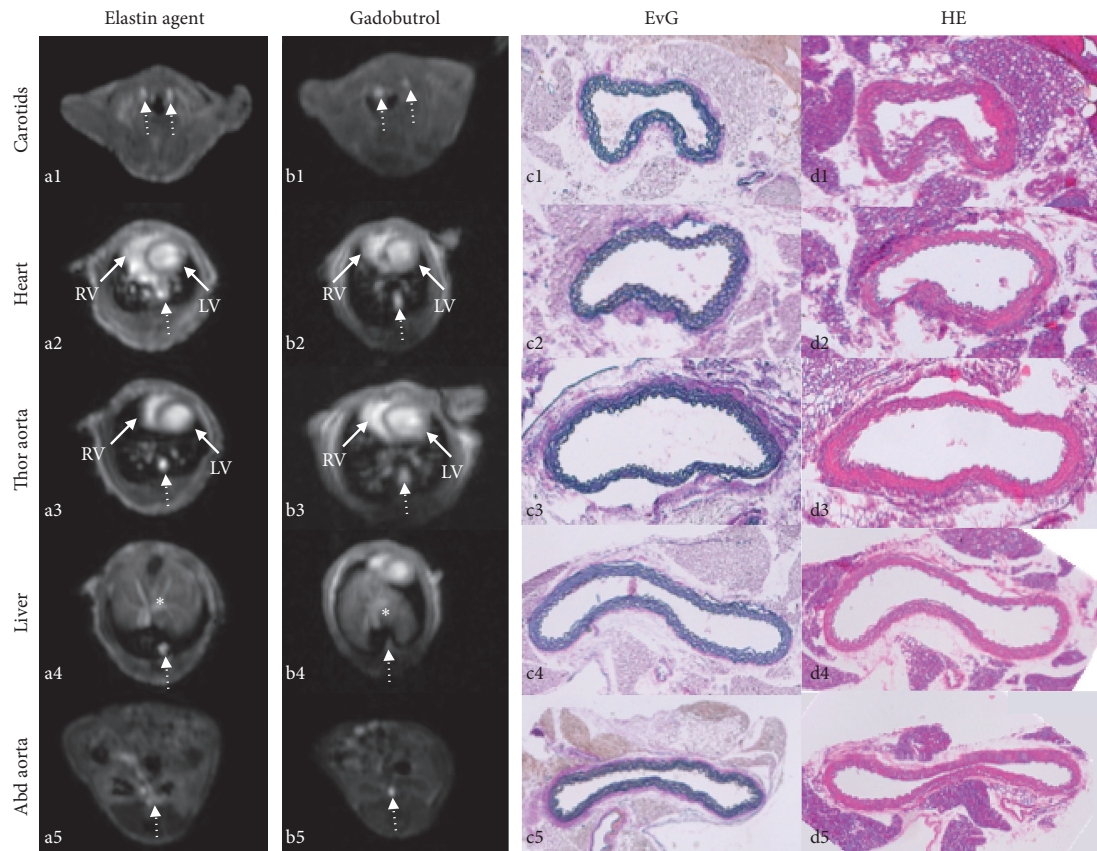


FIGURE 3: Example of a high-resolution 3D angiography (T1 FLASH) following the administration of the elastin-specific molecular agent and the clinically used agent gadobutrol. (a, b) Transversal imaging planes at different anatomical locations demonstrating the visualization of the large vascular structures. (c, d) Corresponding histology at the different locations. (a1, b2) Visualization of the carotid vasculature with the elastin-specific agent and gadobutrol. It can be appreciated that the carotid arteries can be visualized with a comparable enhancement using both probes. (a2, a3 b2, b3) Visualization of the left/right ventricle and thoracic aorta using both probes. (a4, b4) Visualization of the aorta (dotted area) and the hepatic vasculature (*). (a5, b5) Visualization of the abdominal aorta at the level of the kidneys. (c1–c5, d1–d5) Corresponding Elastica van Giesson stain and hematoxylin/eosin stain of the aorta at corresponding levels. EvG: Elastica van Giesson stain; HE: hematoxylin/eosin stain; RV: right ventricle; LV: left ventricle.

3.4. Correlation of In Vivo Angiography with Ex Vivo Histology. *In vivo* and *ex vivo* luminal area measurements were performed in the high-resolution 3D angiography (T1 FLASH) following the administration of the elastin-specific molecular agent and the extracellular extravascular agent gadobutrol (Figures 3(a) and 3(b)). *Ex vivo* area measurements were performed based on the Elastica van Giesson stain (Figure 3(c)). A close and significant correlation was measured between the *in vivo* luminal area following the administration of the elastin-specific molecular agent ($y = 2.26x + 0.59$, $R^2 = 0.87$, $p < 0.05$, Figures 6(a) and 6(b)). Furthermore, a close and significant correlation was measured between the *in vivo* luminal area following the administration of gadobutrol ($y = 2.35x + 0.62$, $R^2 = 0.86$, $p < 0.05$, Figures 6(c) and 6(d)). Small 95% confidence intervals can be seen in the Bland-Altman plots. For the elastin-specific agent, the 95% confidence interval ranged from -1.86 to -0.09 . For gadobutrol, the 95% confidence interval ranged from -2.00

to -0.09 . Overall, measurements of the *in vivo* vascular area were higher compared to measurements of the *ex vivo* vascular area. These smaller size measurements on *ex vivo* histology can be explained by an *in vivo* partial volume effect and tissue shrinkage, which results from the processing of the tissue samples.

4. Discussion

This study demonstrated that a novel elastin-specific molecular probe enables the performance of a contrast-enhanced first-pass and late 3D MR angiography at a clinically relevant dose with an intravascular contrast enhancement and image quality comparable to a clinically used extravascular contrast agent (gadobutrol). All measurements were performed at the same clinical dose of both probes and at a clinical field strength with a clinical sequence design.

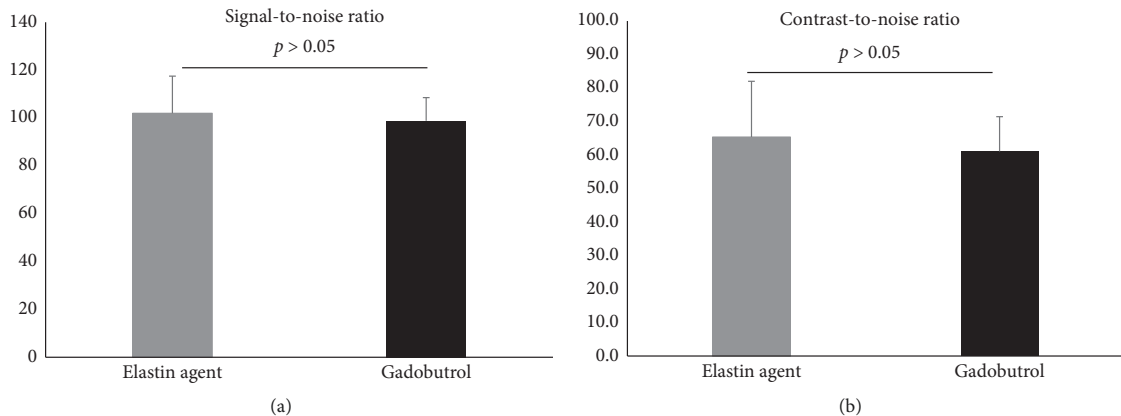


FIGURE 4: Signal-to-noise ratios and contrast-to-noise ratios in the high-resolution 3D angiography (FLASH) following the administration of the elastin-specific molecular agent and the clinically used agent gadobutrol. (a, b) Signal-to-noise and contrast-to-noise ratios of the aorta in the high-resolution 3D angiography (FLASH) following the administration of the elastin-specific molecular agent and the clinically used gadobutrol ($n = 8$). The elastin-specific molecular probe demonstrated a slightly higher signal-to-noise ratio and contrast-to-noise ratio, which was not significantly different from the signal-to-noise ratio and contrast-to-noise ratio of gadobutrol ($p > 0.05$).

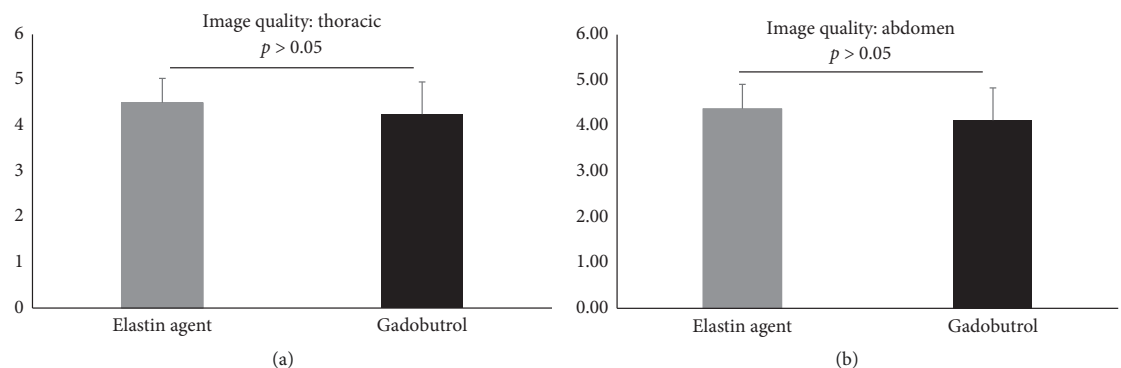


FIGURE 5: Image quality of the high-resolution 3D angiography (FLASH) following the administration of the elastin-specific molecular agent and the clinically used agent gadobutrol. (a, b) Image quality of the vascular system in the high-resolution 3D angiography (FLASH) following the administration of the elastin-specific molecular agent and the clinically used agent gadobutrol ($n = 8$). Both probes showed a high image quality for the visualization of the aorta in the thorax and abdomen with no significant difference between the two probes ($p > 0.05$).

4.1. Biokinetic Properties of the Elastin-Specific Probe. The paramagnetic ^{158}Gd -labelled $\text{C}_{32}\text{H}_{40}\text{N}_7\text{O}_{11}$ (856 Dalton) elastin-specific molecular probe is a low-molecular-weight contrast agent. Comparable to clinically used gadolinium-based contrast agents, the relatively small probe is labelled with a single gadolinium chelate [5]. Because of its small size, this probe shows a rapid clearance from the blood pool, comparable to clinically used first-pass agents. To enable elastin imaging of the molecular target shortly after the intravenous administration, a high target to background ratio was shown to be reached within the first hour [5]. For the elastin-specific agent, the uptake in the target tissue was demonstrated to be the highest at approximately 30 to 45 minutes after injection. Nontarget tissues, such as heart, lung and muscle, showed a low uptake and

rapid washout. The uptake in the liver was shown to be low, indicating that the probe is not primarily excreted via the hepatobiliary system. By contrast, the high measured probe concentration in kidney and urine indicated the rapid renal clearance of the agent. Overall, these properties represent a favourable pharmacokinetic profile of the elastin-specific molecular probe comparable to clinically used gadolinium-based contrast agents, such as gadobutrol.

4.2. Imaging Properties of MR Probes in a Clinical Setting. For the visualization of the vascular system in patients and the characterization of pathologies, different types of MR probes, including gadolinium-based and iron oxide-based agents have

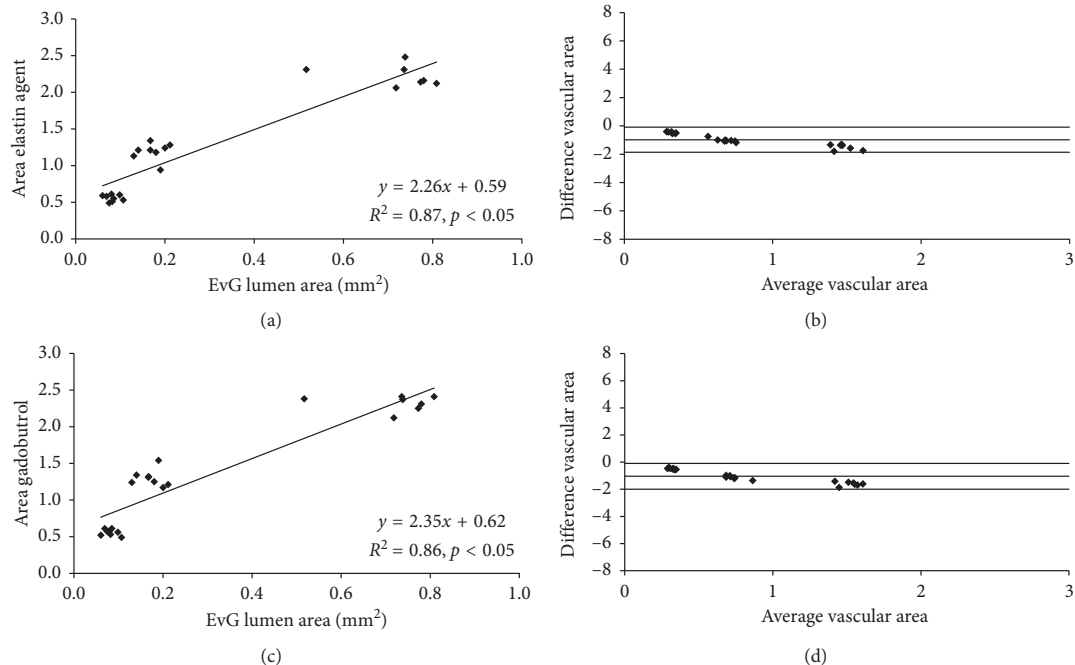


FIGURE 6: Correlation of *in vivo* aortic area measurements following the administration of the probes and the *ex vivo* measurements on the Elastica van Giesson stain. (a) *In vivo* area measurements following the administration of the elastin-specific molecular probe showed a close correlation with the *ex vivo* measurements on the Elastica van Giesson stain ($n = 4$). Measurements were performed on the high-resolution 3D angiography (flash). (b) Bland-Altman analysis only shows a minor difference between the two measurements with relatively small confidence intervals. (c) *In vivo* area measurements following the administration of gadobutrol showed a close correlation with the *ex vivo* measurements on the Elastica van Giesson stain ($n = 4$). (d) Bland-Altman analysis only shows a minor difference between the two measurements with relatively small confidence intervals. EvG: Elastica van Giesson stain.

been investigated [2, 11]. In clinical practice, extravascular gadolinium-based contrast agents are the most commonly used imaging agents for applications, in which contrast enhancement is required. The most important clinical application of these imaging agents is the visualization of the different vascular phases, including the arterial, venous, and delayed phase with a high SNR and CNR. For the evaluation of patients, the most important clinical information for the characterization of pathologies are derived from these phases. If a novel agent probe is introduced into clinical practice, the probe should ideally enable imaging of these clinically important phases. The current clinically used MR contrast agents rapidly extravasate out of the arterial and venous lumen into the extracellular space following the early blood phase. In the context of cardiovascular imaging, current clinically used MR agents have been shown to accumulate in areas with fibrotic tissue, e.g., enabling myocardial scar imaging. However as this is a “passive” process not targeted against a specific protein or cell, they provide only indirect/unspecific and limited information about pathological processes when used for delayed enhancement.

In this study, we investigated the properties of a novel elastin-specific gadolinium-based molecular probe for the visualization of the clinically important early arterial phases. Importantly, all measurements were performed at the same clinically relevant dose (0.1 mmol/kg) with

a single bolus administration. Additionally, all imaging was performed with clinically used MR sequences and at a clinical field strength of 3T. The elastin-specific gadolinium-based molecular probe demonstrated comparable imaging properties to the routinely used clinical contrast agent gadobutrol for the performance of an MR angiography. Following the intravenous injection, both agents were shown to demonstrate a comparable rapid renal clearance from the blood pool. Because of this property, the highest intravascular signal could be achieved during the first-pass following the intravenous administration. Additionally, both agents showed a similar SNR and CNR during the first-pass and a comparable washout pattern, which is in line with previous studies [5–8]. The SNR and CNR derived from the elastin-specific agent was slightly, however not significantly, higher compared to the enhancement derived from gadobutrol. This can be explained by the slightly higher relaxivity of the elastin-specific agent compared to gadobutrol [5, 9].

In summary, this study demonstrated that the elastin-specific molecular probe shows excellent signal properties for the acquisition of time-resolved first-pass and late 3D MR angiographies. Signal enhancement of the aorta was comparable to what was measured with the clinically used agent (gadobutrol) at the same dose. This indicates that first-pass

angiography and tissue perfusion, e.g., for tumor evaluation could be performed with comparable SNR and CNR as with currently used clinical gadolinium-based agents. The main advantage of the elastin-specific probe, compared to unspecific clinically used probes, is that it can also be used for the visualization of specific pathological processes with the expression of (tropo-)elastin in delayed imaging.

4.3. Translation of Results into a Clinical Setting. This study has several advantages regarding the translation of the results into clinical applications: (1) All imaging were performed at a clinically relevant field strength, which allows direct translation to human applications. (2) The MR sequences used in this study are based on a clinical MR imaging protocol. (3) The molecular character and size of the used probe is directly comparable to clinically approved contrast agents, increasing the probability of a translation into clinical applications. Despite the prevalence of high-field scanners in previously published small animals MRI studies, clinical MRI systems are being increasingly used for preclinical research. This study was performed on a clinical 3T MR imaging system for several reasons. The effects on T1 and T2 relaxation, rotational correlation and signal properties of molecular probes, and potential sources of artefacts (fat, air/tissue interfaces) can vary substantially depending on the applied field strength (1.5–3T vs. >7T) and may therefore limit the direct translation of the findings to human application [12]. Additionally, when utilizing a clinical MRI system, protocols and imaging pulse sequences that are already highly optimized for clinical practice, can be adapted and scaled down for preclinical use. Subsequently, these sequences can easily be scaled back for clinical practice. The translation from preclinical to clinical studies is therefore greatly facilitated. 3T is chosen over 1.5T because of the increased SNR and CNR and thus higher spatial resolution achievable. A clinical single-loop microscopy coil was used to achieve the high signal levels needed for high-resolution small animal imaging.

4.4. Limitations. This study has several limitations. The MR probe was evaluated in an experimental small animal study. However, previous experimental studies have shown that this type of study can yield a good indication of how a MR agent could perform in a clinical setting. Secondly, a relatively small number of animals with defined doses of the MR agent was used. Additionally, a single acquisition protocol with a single regime of contrast injection was applied. This acquisition protocol was directly derived from the clinical imaging protocol and scaled down for this study. Imaging was performed only at 3T and therefore the results are not directly applicable to 1.5T scanners.

5. Conclusion

The novel elastin-specific molecular probe enables the performance of a contrast-enhanced first-pass and late 3D

Contrast Media & Molecular Imaging

MR angiography with an intravascular contrast enhancement and image quality comparable to a clinically used extravascular contrast agent.

Data Availability

The data used to support the findings of this study are available from the corresponding author upon request.

Conflicts of Interest

The authors declare that there are no conflicts of interest regarding the publication of this article.

Acknowledgments

This study was supported by the Deutsche Forschungsgemeinschaft (MA 5943/3-1/4-1/9-1). The elastin agent was provided by Lantheus Medical Imaging.

Supplementary Materials

Supplementary Figure 1: (A) example of tubes with diluted gadobutrol of the approximated *in vivo* concentration ranging from 0.00125 mmol per ml to 0.00033 mmol per ml. We imaged with the same imaging set-up and MR sequences as in the *in vivo* experiments. (B) A close correlation of the *ex vivo* SNR and CNR measurements with the overall gadolinium concentration over a wide range of dilutions was found. Additionally, measurements in 3 mm tubes strongly correlated with measurements in 1 mm tubes. Supplementary Figure 2: the red regions indicate the region of interest (ROI) used for the assessment of the signal from the left ventricle. (A, B) The images show the first-pass MR angiography (TWIST) following the administration of the elastin agent and the clinically used agent gadobutrol. (A1, B1) Precontrast images at the level of the heart showed no relevant signal enhancement prior to the administration of the probes. (A2, B2) Immediately after the administration of the imaging agents, a high signal in the left and right ventricle can be appreciated during the first-pass. Visually, the signal intensity from both probes was comparable. (A3, B3) 30 seconds after the administration of the probes, a clear reduction of the signal at the level of the heart can be appreciated. (A4, B4) 60 seconds following the administration of the probes, a further decrease in signal can be appreciated. RV: right ventricle, LV: left ventricle. (*Supplementary Materials*)

References

- [1] T. Chandra, B. Pukenas, S. Mohan, and E. Melhem, "Contrast-enhanced magnetic resonance angiography," *Magnetic Resonance Imaging Clinics of North America*, vol. 20, no. 4, pp. 687–698, 2012.
- [2] M. R. Prince and J. F. Meaney, "Expanding role of MR angiography in clinical practice," *European Radiology Supplements*, vol. 16, no. 2, pp. B3–B8, 2006.
- [3] I. S. Tuna and S. Tatli, "Contrast-enhanced CT and MR imaging of renal vessels," *Abdominal Imaging*, vol. 39, no. 4, pp. 875–891, 2014.

Contrast Media & Molecular Imaging

9

- [4] M. Voth, S. Haneder, K. Huck et al., "Peripheral magnetic resonance angiography with continuous table movement in combination with high spatial and temporal resolution time-resolved MRA with a total single dose (0.1 mmol/kg) of gadobutrol at 3.0 T," *Investigative Radiology*, vol. 44, no. 9, pp. 627–633, 2009.
- [5] M. R. Makowski, A. J. Wiethoff, U. Blume et al., "Assessment of atherosclerotic plaque burden with an elastin-specific magnetic resonance contrast agent," *Nature Medicine*, vol. 17, no. 3, pp. 383–388, 2011.
- [6] M. R. Makowski, A. Preissel, C. von Bary et al., "Three-dimensional imaging of the aortic vessel wall using an elastin-specific magnetic resonance contrast agent," *Investigative Radiology*, vol. 47, pp. 438–444, 2012.
- [7] R. M. Botnar, A. J. Wiethoff, U. Ebersberger et al., "In vivo assessment of aortic aneurysm wall integrity using elastin-specific molecular magnetic resonance imaging," *Circulation: Cardiovascular Imaging*, vol. 7, no. 4, pp. 679–689, 2014.
- [8] H. Okamura, L. J. Pisani, A. R. Dalal et al., "Assessment of elastin deficit in a Marfan mouse aneurysm model using an elastin-specific magnetic resonance imaging contrast agent," *Circulation: Cardiovascular Imaging*, vol. 7, no. 4, pp. 690–696, 2014.
- [9] J. Pintaske, P. Martirosian, H. Graf et al., "Relaxivity of gadopentetate dimeglumine (Magnevist), gadobutrol (Gadovist), and gadobenate dimeglumine (MultiHance) in human blood plasma at 0.2, 1.5, and 3 Tesla," *Investigative Radiology*, vol. 41, pp. 213–221, 2006.
- [10] M. V. McConnell, V. C. Khasgiwala, B. J. Savord et al., "Comparison of respiratory suppression methods and navigator locations for MR coronary angiography," *American Journal of Roentgenology*, vol. 168, no. 5, pp. 1369–1375, 1997.
- [11] J. P. Finn, K. L. Nguyen, F. Han et al., "Cardiovascular MRI with ferumoxytol," *Clinical Radiology*, vol. 71, no. 8, pp. 796–806, 2016.
- [12] C. T. Farrar, G. Dai, M. Novikov et al., "Impact of field strength and iron oxide nanoparticle concentration on the linearity and diagnostic accuracy of off-resonance imaging," *NMR in Biomedicine*, vol. 21, no. 5, pp. 453–463, 2008.

2.2 Dual-probe molecular MRI for the *in vivo* characterization of atherosclerosis in a mouse model: Simultaneous assessment of plaque inflammation and extracellular-matrix remodeling

Autoren: Carolin Reimann, Julia Brangsch, Jan O. Kaufmann, Lisa C. Adams, David C. Onthank, Christa Thöne-Reineke, Simon P. Robinson, Bernd Hamm, Rene M. Botnar, Marcus R. Makowski

Jahr: 2019

Journal: Scientific Reports

Published: 2019; Sept. 25. doi: 10.1038/s41598-019-50100-8

Bibliografische Quelle: Reimann C, Brangsch J, Kaufmann JO, Adams LC, Onthank DC, Thone-Reineke C, Robinson SP, Hamm B, Botnar RM, Makowski MR. Dual-probe molecular MRI for the *in vivo* characterization of atherosclerosis in a mouse model: Simultaneous assessment of plaque inflammation and extracellular-matrix remodeling. *Scientific reports.* 2019;9(1):13827

Received: 17 May 2019

Accepted: 3 September 2019

Published online: 25 September 2019

OPEN

Dual-probe molecular MRI for the *in vivo* characterization of atherosclerosis in a mouse model: *Simultaneous assessment of plaque inflammation and extracellular-matrix remodeling*

Carolin Reimann^{1,2}, Julia Brangsch^{1,2}, Jan O. Kaufmann^{1,3,4}, Lisa C. Adams¹, David C. Onthank⁵, Christa Thöne-Reineke¹, Simon P. Robinson⁵, Bernd Hamm¹, Rene M. Botnar^{1,6,7,8,9} & Marcus R. Makowski^{1,6,8}

Molecular MRI is a promising *in-vivo* modality to detect and quantify morphological and molecular vessel-wall changes in atherosclerosis. The combination of different molecular biomarkers may improve the risk stratification of patients. This study aimed to investigate the feasibility of simultaneous visualization and quantification of plaque-burden and inflammatory activity by dual-probe molecular MRI in a mouse-model of progressive atherosclerosis and in response-to-therapy. Homozygous apolipoprotein E knockout mice ($\text{ApoE}^{-/-}$) were fed a high-fat-diet (HFD) for up to four-months prior to MRI of the brachiocephalic-artery. To assess response-to-therapy, a statin was administered for the same duration. MR imaging was performed before and after administration of an elastin-specific gadolinium-based and a macrophage-specific iron-oxide-based probe. Following *in-vivo* MRI, samples were analyzed using histology, immunohistochemistry, inductively-coupled-mass-spectrometry and laser-inductively-coupled-mass-spectrometry. In atherosclerotic-plaques, intraplaque expression of elastic-fibers and inflammatory activity were not directly linked. While the elastin-specific probe demonstrated the highest accumulation in advanced atherosclerotic-plaques after four-months of HFD, the iron-oxide-based probe showed highest accumulation in early atherosclerotic-plaques after two-months of HFD. *In-vivo* measurements for the elastin and iron-oxide-probe were in good agreement with *ex-vivo* histopathology (Elastica-van-Gieson stain: $y = 298.2 + 5.8$, $R^2 = 0.83$, $p < 0.05$; Perl's Prussian-blue-stain: $y = 834.1 + 0.67$, $R^2 = 0.88$, $p < 0.05$). Contrast-to-noise-ratio (CNR) measurements of the elastin probe were in good agreement with ICP-MS ($y = 0.11x - 11.3$, $R^2 = 0.73$, $p < 0.05$). Late stage atherosclerotic-plaques displayed the strongest increase in both CNR and gadolinium concentration ($p < 0.05$). The gadolinium probe did not affect the visualization of the iron-oxide-probe and vice versa. This study demonstrates the feasibility of simultaneous assessment of plaque-burden

¹Charité – Universitätsmedizin Berlin, corporate member of Freie Universität Berlin, Humboldt-Universität zu Berlin, and Berlin Institute of Health, Charitéplatz 1, 10117, Berlin, Germany. ²Department of Veterinary Medicine, Institute of Animal Welfare, Animal Behavior and Laboratory Animal Science, Freie Universität Berlin, Königs weg 67, Building 21, 14163, Berlin, Germany. ³Federal Institute for Materials Research and Testing (BAM), Division 1.5 Protein Analysis, Richard-Willstätter-Str. 11, 12489, Berlin, Germany. ⁴Humboldt-Universität Berlin, Department of Chemistry, Brook-Taylor-Str. 2, 12489, Berlin, Germany. ⁵Lantheus Medical Imaging, North Billerica, Massachusetts, 331 Treble Cove Road, USA. ⁶King's College London, School of Biomedical Engineering and Imaging Sciences, St Thomas' Hospital Westminster Bridge Road, London, SE1 7EH, United Kingdom. ⁷Wellcome Trust/EPSRC Centre for Medical Engineering, King's College London, London, United Kingdom. ⁸BHF Centre of Excellence, King's College London, London, United Kingdom. ⁹Escuela de Ingeniería, Pontificia Universidad Católica de Chile, Santiago, Chile. Correspondence and requests for materials should be addressed to C.R. (email: Carolin.Reimann@charite.de)

www.nature.com/scientificreports/

and inflammatory activity by dual-probe molecular MRI of progressive atherosclerosis. The *in-vivo* detection and quantification of different MR biomarkers in a single scan could be useful to improve characterization of atherosclerotic-lesions.

Atherosclerosis is the leading cause of morbidity and mortality in the Western world and developing countries¹. The development of atherosclerosis is a complex process with a dynamic influx of proinflammatory cells and a progressive increase of plaque-burden, which is associated with de-novo synthesis of extracellular-matrix proteins².

Atherosclerosis progresses relatively slowly and, in most cases, remains asymptomatic until the end-stage of the disease. Sudden surface erosion or plaque rupture can lead to vascular occlusion and ischemia, resulting in myocardial infarction or cerebral stroke³.

In a clinical setting, conventional angiographic techniques are used to assess the degree of luminal narrowing in the coronary and carotid-arteries⁴. Even though angiographic techniques are the diagnostic reference standard, there is growing evidence, that the interventional treatment of the atherosclerotic-plaque, associated with the highest degree of stenosis, does not improve the prognosis in all patients⁵. Furthermore, previous research demonstrated that the highest number of ruptured atherosclerotic-plaques were found in arteries with <60% of stenosis⁶.

Substantial progress has been made with invasive and non-invasive imaging methods in the quest for the “vulnerable plaque” in recent years. It is well established, that features of vulnerable plaques go beyond the severity of vascular stenosis⁷. There is a combination of plaque features, which are strongly associated with plaque vulnerability, including the influx of proinflammatory cells, positive vascular-remodeling, angiogenesis, a large necrotic core, a thin fibrotic cap, micro-calcifications and plaque hemorrhage.

In this context several invasive and noninvasive imaging techniques have been investigated, but none has been widely adopted in clinical practice.

Inflammatory activity and plaque-burden, which can both be visualized by molecular MRI techniques, were established as key features of vulnerable atherosclerotic-plaques. Therefore, the combined assessment of two different plaque characteristics in one scan has the potential to improve the stratification of patients at risk for myocardial infarction or cerebral stroke⁸. So far, a combined assessment of two features (inflammatory activity, plaque-burden) in a single scan has not been established in the context of atherosclerosis. This study aimed to investigate the feasibility of a simultaneous characterization of the plaque-burden and inflammatory activity by dual-probe molecular MRI in a mouse-model of progressive atherosclerosis and in response-to-therapy. For the visualization of the extracellular-matrix we used a gadolinium-based elastin-specific agent, for the visualization of proinflammatory cells we used a clinically approved iron-oxide agent Feraheme (Ferumoxytol, AMAG-Pharmaceuticals, Waltham, MA, USA). There are a couple of applications with simultaneous use of Gd-based and iron-oxide -based imaging probes. They demonstrate that high-resolution magnetic resonance imaging (MRI) allows combining cellular-scale resolution with the ability to detect two cell types simultaneously at any tissue depth^{9,10}.

Materials and Methods

Animals. This study was performed according the local guidelines and provisions for the implementation of the Animal Welfare Act and regulations of the Federation of Laboratory Animal Science Associations (FELASA). The regulatory authority the Regional Office for Health and Social Affairs Berlin (LAGeSo) approved this animal study. We used eight weeks old apolipoprotein-E-deficient ($\text{ApoE}^{-/-}$) male mice. $\text{ApoE}^{-/-}$ mice were fed with a high-fat-diet (HFD) containing 21% fat from lard, supplemented with 0.15% (wt/wt) cholesterol (Special-Diets-Services, Witham, UK) at the age of two-months. A control group with nine 26 week old male C57BL/6J mice was used. Statin-treatment was performed in a subgroup of $\text{ApoE}^{-/-}$ mice ($n = 9$) and started in parallel with the feeding of the HFD feeding. Pravastatin (Kemprotec-Limited, Middlesbrough, UK) was administered at a dose of 40 mg/kg body-weight/day via drinking water. Please refer to Supplementary Fig. 1 for the experimental setup and for further details to the Supplementary Material.

Gadolinium-based elastin-specific agent. In this study we used a low molecular weight gadolinium-based (856 g/mol molecular-mass) elastin-specific MR agent. A rapid clearance from the blood-pool via the kidneys and highest binding can be measured 30 to 45 minutes following the administration^{11,12}. For the unbound and bound agent, a longitudinal-relaxivity of $4.68 \pm 0.13 \text{ mM}^{-1}\text{s}^{-1}$ and $8.65 \pm 0.42 \text{ mM}^{-1}\text{s}^{-1}$ was reported, which is higher than for clinical used agents, such as gadobutrol^{11,12}. This probe was validated and used in different previous studies to visualize the extracellular-matrix (ECM) protein, elastin^{11,12}. The *in-vivo* visualization of the ECM protein elastin in atherosclerotic-plaque represents a surrogate marker for overall plaque-burden^{11,12}. In this study, the elastin-specific probe was administered *via* the tail vein at a clinically used dose of 0.2 mmol/kg on days one of MRI examination and after 24 h on day two of MRI examination.

Iron-oxide-based macrophage-specific agent. The iron-oxide-particle used in this study is coated with semisynthetic carbohydrate (ferumoxytol). Because of its effectiveness in shortening T1 and T2 relaxation times this agent was developed as a MRI agent initially¹³. Ferumoxytol (Feraheme®, AMAG-Pharmaceuticals, Waltham, MA, USA) was approved by the Food-and-Drug-Administration (FDA) for iron-deficiency-anemia treatment in adults with chronic-kidney- disease (CKD) in 2009. In recent years the use of off-label iron-oxide nanoparticle as a MRI probe by clinicians and researchers has grown¹³. A linear dependence of R1, R2, and R2* on ferumoxytol concentration was found in saline and plasma with lower R1 values at 3.0 T and similar R2 and R2* values at 3.0 T ($r1_{\text{saline}} = 10.0 \pm 0.3 \text{ s}\text{mM}$; $r1_{\text{plasma}} = 9.5 \pm 0.2 \text{ s}\text{mM}$; $r2_{\text{saline}} = 62.3 \pm 3.7 \text{ s}\text{mM}$; $r2_{\text{plasma}} = 65.2 \pm 1.8 \text{ s}\text{mM}$; $r2^*_{\text{saline}} = 57.0 \pm 4.7 \text{ s}\text{mM}$; $r2^*_{\text{plasma}} = 55.7 \pm 4.4 \text{ s}\text{mM}$)¹⁴. In this study, ferumoxytol was administered at the clinical dose (4 mg Fe/kg) *via* the tail vein injection and imaging was performed after 24-hours.

www.nature.com/scientificreports/

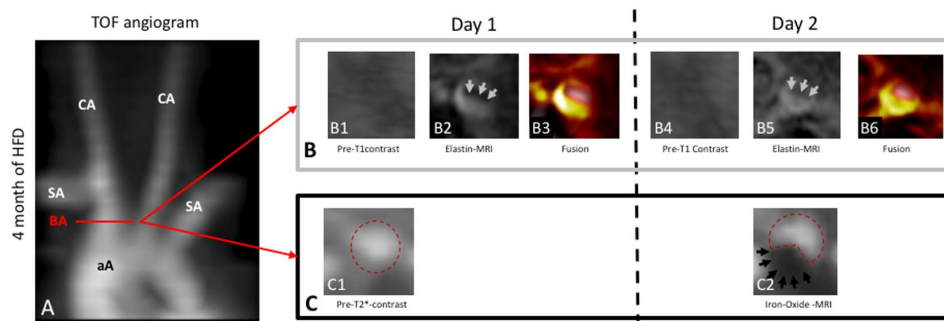


Figure 1. Multitarget characterization of the plaque-burden and inflammatory activity by molecular MRI. (A) Time-of-flight-angiography showing the aortic-arch, brachiocephalic-artery, subclavian-artery and carotid-arteries of an ApoE^{-/-} mice after four-months of high-fat-diet. (B) T1-weighted-imaging pre-contrast (B1, B4) and following the administration of the gadolinium-based elastin-specific MR-probe (B2, B5) at the clinical dose of 0.2 mmol/kg. Automatic image-fusion (B3, B6) demonstrates the localization of the signal from the MR-probe in the vascular-wall in relation to the blood signal (B4). (C) T2*-weighted-imaging prior to and following the administration of the iron-oxide-probe (ferumoxytol) at the clinical dose of 4 mg Fe/kg. On pre-contrast images, the vascular lumen can be clearly delineated for circular shape (C1). 24-hours following the administration of the iron-oxide-particle, a clear signal-void reduces the signal from the lumen can be visualized (C2), reflecting the accumulation of the iron-oxide-particles in atherosclerotic-plaques.

In-vivo MR Experiments. Imaging sessions were performed at a clinical 3T Siemens system (Biograph, Siemens Healthcare, Erlangen, Germany) with a single loop coil (diameter 4 cm) with mice in prone position. For details regarding the T1-weighted and T2*-weighted sequences please refer to the Supplementary Material.

Assessment of magnetic resonance imaging signal. Evaluation of the gadolinium-based elastin-specific probe on T1-weighted sequences. The quantification of the MRI signal was conducted using OsiriX (OsiriX Foundation, Geneva, Version5.6). To assess the lumen and arterial-wall including the atherosclerotic-plaque, time-of-flight (TOF) images were automatically co-registered and overlaid with high-resolution MRI images. Morphometric measurements were implemented on high-resolution MRI images. Regions of interest (ROIs) were co-localized with the atherosclerotic-plaque (highest signal within the arterial wall) and defined as areas of enhancement on high-resolution MRI images. We calculated the contrast-to-noise-ratio with following equation: CNR = (Combined vessel-wall and atherosclerotic-tissue-signal – Blood-signal)/Noise. The noise was defined as the standard deviation in pixel intensity from a ROI placed in the background air anterior to brachiocephalic-artery.

Quantification of iron-oxide on T2*-weighted sequences. MR images of the vessel-lumen areas were compared between pre-contrast T2*-weighted MR images prior and iron-oxide injection 24 h post injection. All data originated from T2*-weighted images are demonstrated the signal-loss area (%) in relating to the pre-contrast MRI scan. To compare areas of signal-void within the ROI identical window and level settings were used. The areas were established semi-automatically using identic 2D-segmentation parameters.

Histological analysis and immunofluorescence of the arterial vessel system and plaque morphometry. Please refer to the Supplementary Material.

Inductively coupled mass spectrometry for quantification of gadolinium and iron and Laser-inductively-coupled-mass-spectrometry (LA ICP-MS) for spatial localization of gadolinium. Please refer to the Supplementary Material.

Competition experiments. Please refer to the Supplementary Material.

Statistical analysis. Please refer to the Supplementary Material.

Results

Multi-target plaque characterization in a single MR imaging session. Simultaneous imaging of the elastin-specific gadolinium-based probe and the macrophage-specific iron-oxide-based probe. This study demonstrates that MR plaque-imaging with two probes can be performed in a single imaging session (Fig. 1). Using a combination of gadolinium-based elastin-specific imaging and iron-oxide-based macrophage-specific imaging different phases of atherosclerotic-plaque development and response-to-therapy could be evaluated. More specifically, de novo synthesis of elastic-fibers and inflammatory activity were not directly linked in atherosclerotic-plaques. In the early-stage of plaque development after two-months of high-fat-diet, only a small increase in de-novo elastin synthesis was observed (14% of the maximum after four-months of high-fat-diet) in the atherosclerotic-plaque. In contrast, a marked increase in iron-oxide-particle accumulation was measured (45% of

www.nature.com/scientificreports/

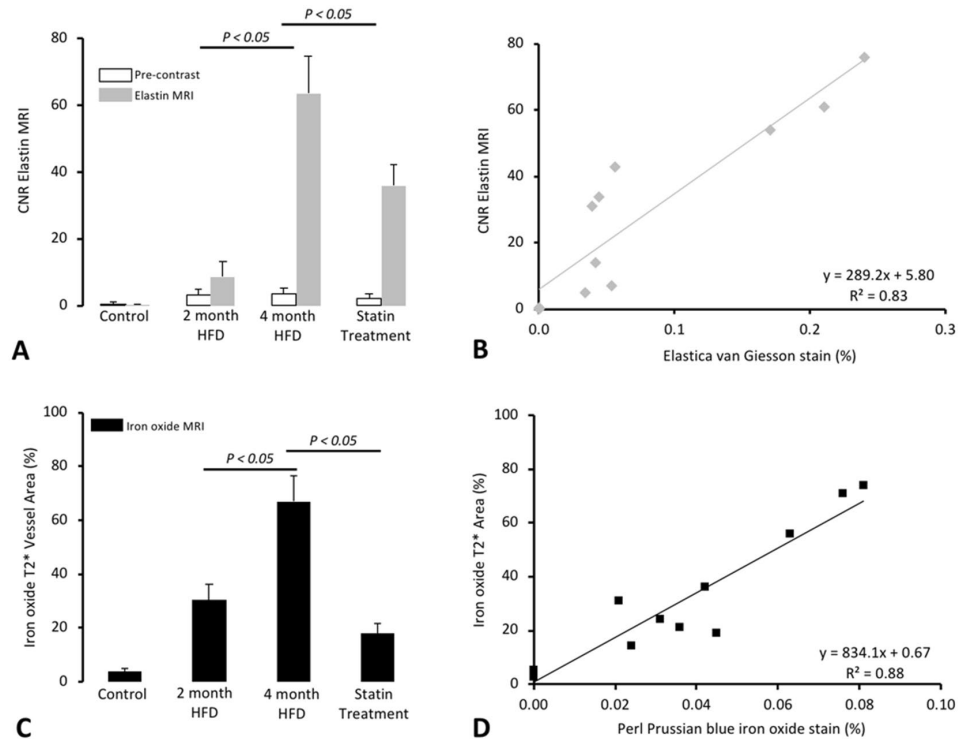


Figure 2. *In vivo* MRI signal measurements and *ex vivo* quantification of gadolinium-based and iron-oxide-based molecular probes. (A) Average atherosclerotic-plaque CNR pre-contrast and following the administration of the gadolinium-based elastin-specific MR-probe. After the injection of the elastin-specific probe, a small increase ($p \leq 0.05$) in atherosclerotic-plaque CNR could be observed, while a strong increase in plaque CNR could be observed after four-months of HFD. (B) In the scatter-plot, the *in vivo* measured CNR showed a strong correlation ($p \leq 0.05$) with the *ex vivo* Elastica-van-Gieson-staining. (C) After two-months of high-fat-diet a strong accumulation ($p \leq 0.05$) of iron-oxide-particles could be observed. After four-months of high-fat-diet, the most pronounced peak ($p \leq 0.05$) was measured. In response to the statin-treatment, a strong reduction ($p \leq 0.05$) in iron-oxide-particle accumulation. (D) In the scatter-plot, the *in vivo* measured signal-void resulting from the iron-oxide-particles showed a strong correlation ($p \leq 0.05$) to the *ex vivo* Perls'-Prussian-blue-stain.

maximum after four-months of high-fat-diet), indicating a strong inflammatory response in the early-stage of the disease. In advanced atherosclerotic-plaques, the influx of macrophages was most pronounced after four-months of high-fat-diet and in the most advanced plaques. In agreement with this abundant deposition of elastic-fibers in the plaque matrix was measured. This indicates, that in advanced plaques strong ECM-remodeling is accompanied by a large influx of pro-inflammatory macrophages.

In response to statin-treatment a different relative response was measured regarding the expression of elastic-fibers and the influx of macrophages. The amount of elastin detectable with ESMA was decreased by 43% compared to the four-months high-fat-diet group, while the influx of macrophages showed an even more pronounced decrease of 73% compared to the four-months high-fat-diet group.

T1-weighted MR imaging for the assessment of the gadolinium-based elastin-specific MR-probe. In all mice, including those on high-fat-diet and the statin-treatment, a low CNR was measured in the brachiocephalic vessel-wall at all time-points on non-contrast-enhanced (pre-contrast) MR scans (Fig. 2A). A minor increase in CNR was measured in the two-months' scans and a strong increase in the four-months' scans. After administration of the elastin-specific MR-probe (Fig. 2A). The measured CNR (Fig. 2A) was lower for mice with the statin treatment and differed to the non-treated four-months-HFD mice. A strong correlation was measured between the CNR and the density of elastic-fibers on Elastica-von-Gieson-staining in the atherosclerotic-plaque ($y = 289.2x + 5.8$, $R^2 = 0.83$, $p \leq 0.05$, Fig. 2B).

T2*-weighted MR imaging for the assessment of macrophage-specific iron-oxide-particles. ApoE^{-/-} and control mice cross-sectional T2*-weighted images of brachiocephalic-artery demonstrated a circulary lumen prior to the administration of the iron-oxide contrast agent ferumoxytol (Fig. 1). Increasing regions of signal-loss were detected in brachiocephalic-plaques in ApoE^{-/-} mice on two and four-months of HFD after 24-hours after ferumoxytol injection. Area of signal-loss was continuous and

www.nature.com/scientificreports/

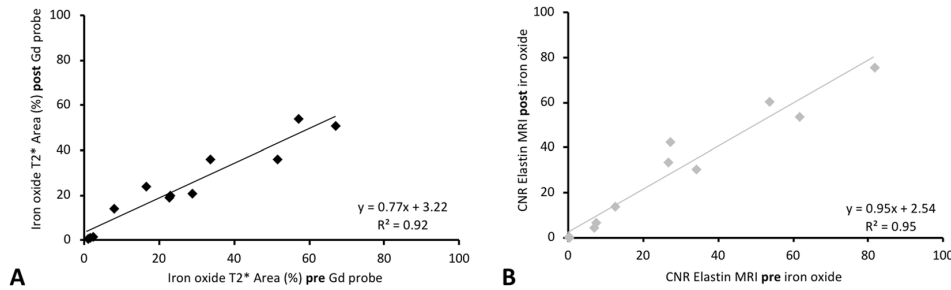


Figure 3. Influence of the gadolinium-based elastin-specific probe on the visualization of iron-oxide-particles and vice versa. If a multi-target approach is chosen, it is of high clinical importance, that the respective imaging probes do not affect the measurements on the other probe. (A) To investigate the influence of iron-oxide-particles on the assessment of the elastin-specific-agent on T1-weighted images, imaging was performed on day one prior to the administration of the iron-oxide-particles and 24-hours following the administration of the iron-oxide-particles. CNR-measurements of the elastin-specific MR-probe showed a strong correlation between both days. (B) To investigate the influence of the gadolinium-based probe on the assessment of the iron-oxide-particles on T2*-weighted-sequences, imaging was performed on day two prior to and following the administration of the elastin-specific probe. The assessment of the effect of iron-oxide-particles on T2*-weighted images prior to the administration of the gadolinium-based probe demonstrated a strong correlation with measurements following the administration of the gadolinium-based probe.

constituted a substantial percentage of the luminal area. There was no effect detected in the control group. After two and four-months of HFD an increase in percent signal-loss (relative to pre-contrast MRI) was detected with plaque-progression ($26.7 \pm 8.3\%$, $47 \pm 9.6\%$, $p \leq 0.05$). Less pronounced signal-loss was detected in the statin treatment group compared to animals on four-months of HFD ($18 \pm 3.6\%$, $p \leq 0.05$). A strong correlation existed between the area loss on T2* and the accumulation of the iron-oxide-particles on Perl's staining ($y = 834.1x + 0.7$, $R^2 = 0.88$, $p \leq 0.05$, Fig. 2D).

Influence of the gadolinium-based elastin-specific probe on the visualization of iron-oxide-particles and vice versa. When using a dual-probe approach, it is of high clinical importance that the gadolinium-based and iron-oxide-based probe do not affect the visualization and quantification of the respective other probe. Therefore, we evaluated the influence of the gadolinium-based probe on the assessment of iron-oxide-particle measurements. 24-hours after the administration of the iron-oxide-particle T2*-weighted-imaging was performed prior to and 45 min following a dose of the elastin-specific probe in animals after four-months of high-fat-diet ($n = 9$). The assessment of iron-oxide-particles on T2*-weighted images prior to a dose of the gadolinium-based probe demonstrated a strong correlation with measurements following a dose of the gadolinium-based probe ($y = 0.77x + 3.2$, $R^2 = 0.92$, $p \leq 0.05$, Fig. 3A). Between both acquisitions no significant differences ($p > 0.05$) were measured. To investigate the influence of the iron-oxide-particles on the assessment of the elastin-specific agent on T1-weighted images, imaging was performed on day one prior to and 24-hours following the administration of the iron-oxide-particles ($n = 9$). The CNR measurements of elastin-specific MR-probe showed a strong correlation between both days ($y = 0.95x + 2.54$, $R^2 = 0.94$, Fig. 3B). Between both days no significant difference ($p > 0.05$) was measured. This indicates that the gadolinium-based and iron-oxide-based probe do not affect the visualization and quantification of the respective other probe at these time-points.

Histology and Immunofluorescence. *Elastin in the extracellular-matrix.* Ex-vivo measurements on histological slices were in good agreement with in-vivo measurements using the elastin-specific probe ($y = 289.2x + 5.8$, $R^2 = 0.83$, $p \leq 0.05$). After two-months of high-fat-diet, a slight, but already significant ($p \leq 0.05$) gain in signal was measured (Fig. 2). After four-months of high-fat-diet, the increase in elastic-fibers in the extracellular matrix of the atherosclerotic-plaque was even stronger ($p \leq 0.05$) (Fig. 2) but in response to the statin-treatment, a significant ($p \leq 0.05$) decrease in the expression of elastic-fibers was observed (Fig. 2).

Macrophages in the atherosclerotic-plaque. To demonstrate the presence of macrophages in the atherosclerotic-lesions a CD68 staining was used (Fig. 4D1–4). With increasing duration of the HFD an increase in %macrophages and %Perls' Prussian-blue-staining ($R^2 = 0.88$, $p \leq 0.05$) was observed (Fig. 2D). In the statin-group, a significant ($p \leq 0.05$) decrease in positive macrophages areas was measured, which was in agreement with a intense decrease in areas positive for iron. Perls' Prussian-blue-stain was negative for iron-oxide depositions without a prior iron-oxide injection in mice four-months on HFD.

Gadolinium concentration by inductively-coupled mass-spectrometry (ICP-MS). From early to advanced phases of disease progression the average concentration of gadolinium in the brachiocephalic-artery wall gained substantially ($n = 15$, Fig. 5). A significant correlation between ex-vivo measured gadolinium concentrations (ICP-MS) and CNR ($p < 0.05$) was found (Fig. 5A). Also, for iron-oxide-particles, a significant

www.nature.com/scientificreports/

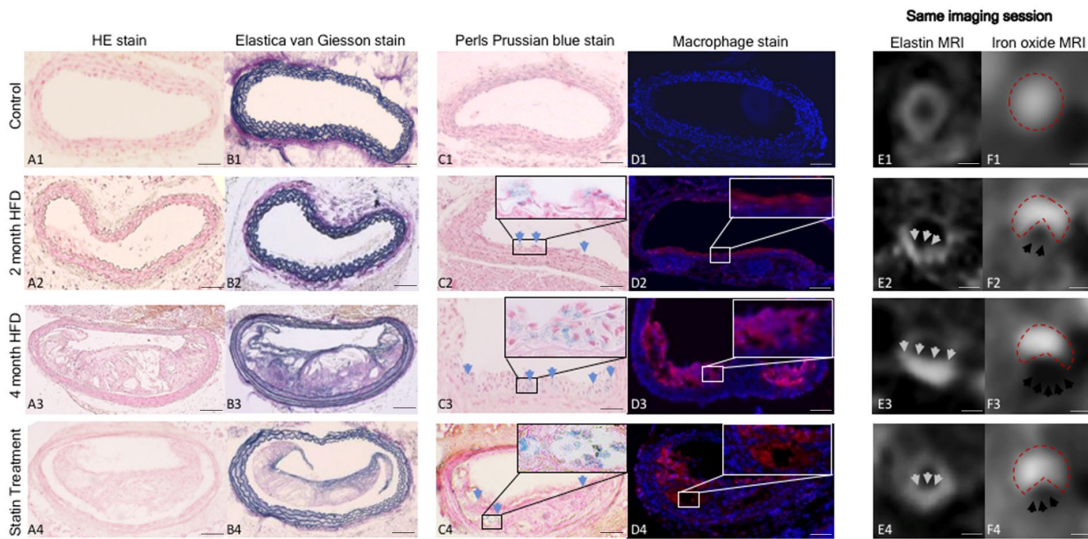


Figure 4. Multitarget characterization of the plaque-burden and inflammatory activity by molecular MRI at different phases of plaque development and in response-to-therapy. (A–C) Cross-sectional histological/immunofluorescence sections (A1–4: Elastica-van-Gieson stain, B1–4: Perls'-Prussian-blue-stain, C1–4: Immunofluorescence-macrophage-stain) of brachiocephalic-arteries of control and ApoE^{-/-} mice two-months, four-months of HFD and statin-treatment. (D,E) T1 and T2*-weighted-imaging with corresponding histology. D1–4: On T1-weighted sequences, a significant increase of vessel-wall-enhancement is in the vessel wall, corresponding to an increased elastin deposition in atherosclerotic-plaque after four-months of HFD. Only a slight increase can be visualized after two-months and following statin-treatment. E1–4: A pronounced signal-void can already be seen after two-months of high-fat-diet, reflecting an already pronounced accumulation of iron-oxide-particles in the atherosclerotic-plaque. The most pronounced signal-void can be observed after four-months of high-fat-diet with almost 50% of the vascular lumen affected by the signal-void. Following statin-treatment, a comparable signal-void to the two-months group is visualized. (A–D) Scale corresponds to 100 µm. (E,F) Scale corresponds to 500 µm.

correlation between the absolute iron-oxide quantity in the brachiocephalic-artery by ICP-MS and T2* measurements ($R^2 = 0.73$, $p < 0.05$, Fig. 5B) was observed.

Spatial localization of the gadolinium-based elastin-specific probe using laser coupled mass spectrometry (LA-ICP-MS). We investigated arterial-wall samples of animals after four-months of high-fat-diet ($n = 3$) and mapped the dispersion of the gadolinium by LA-ICP-MS to define the gadolinium dispersion within the arterial-wall after the administration of the elastin-specific probe. Co-localization of targeted gadolinium with elastic-fibers was determined (Fig. 6B, $n = 3$).

Competition experiments. To reaffirm the specific binding of the elastin-specific molecular agent an *in-vivo* competition experiment was performed. A pre-injection of a tenfold-higher-dose of non-paramagnetic-europium-labeled elastin-specific MR-probe resulted in a distinct decrease of CNR differs to the application of the gadolinium-labeled elastin-specific agent. Between pre-contrast scans on days one and two no significant differences were measured. The *in-vivo* competition experiments were performed in ApoE^{-/-} mice ($n = 3$) on a four-month's high-fat-diet (Fig. 6A).

Discussion

This study demonstrates the feasibility of multi-probe molecular MRI for the simultaneous characterization of extracellular-matrix remodeling and inflammatory activity in a mouse-model of progressive atherosclerosis. There was a temporal delay between de-novo synthesis of elastic-fibers and inflammatory activity in atherosclerotic-plaques. While inflammation was more pronounced in early atherosclerotic-plaques and showed a stronger response to statin therapy, elastin deposition was highest in advanced atherosclerotic-plaques.

This is the first *in-vivo* MR study to demonstrate that both ECM-remodeling and inflammation can be visualized and quantified using a multi-probe approach in a single MR examination. Additionally, it was demonstrated that the gadolinium-based and iron-oxide-based probe do not affect each other and thus visualization and quantification of the respective targets was not compromised.

The simultaneous *in-vivo* detection and quantification of inflammation and ECM-remodeling could be useful for an improved characterization and staging of coronary and carotid atherosclerotic-lesions, which may aid *in-vivo* characterization of the disease, including the assessment of response-to-therapy.

www.nature.com/scientificreports/

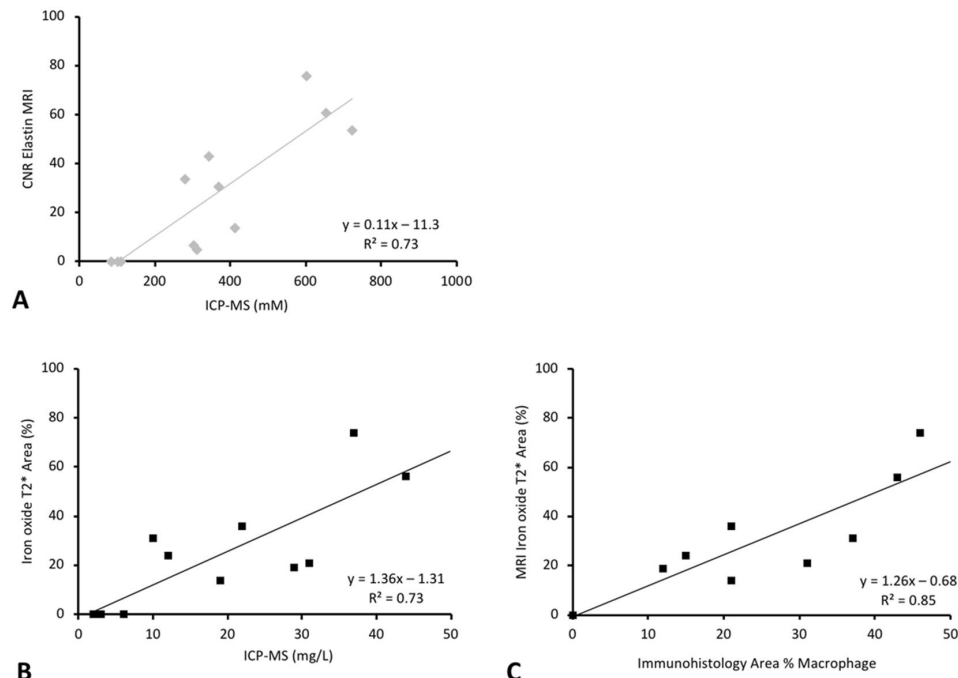


Figure 5. *In vivo* MRI signal measurements and *ex vivo* quantification of molecular probes. (A) The scatter-plots show a strong correlation between *in vivo* CNR and results from ICP-MS of brachiocephalic-arteries. (B) The scatter-plot shows a strong correlation between the signal-void on the T2*-weighted-sequences with the results from ICP-MS. (C) The immunofluorescence-staining of the macrophage area using an antibody (CD68-Antibody) cause a strong correlation ($p \leq 0.05$) with the signal-void on the T2*-weighted-sequences.

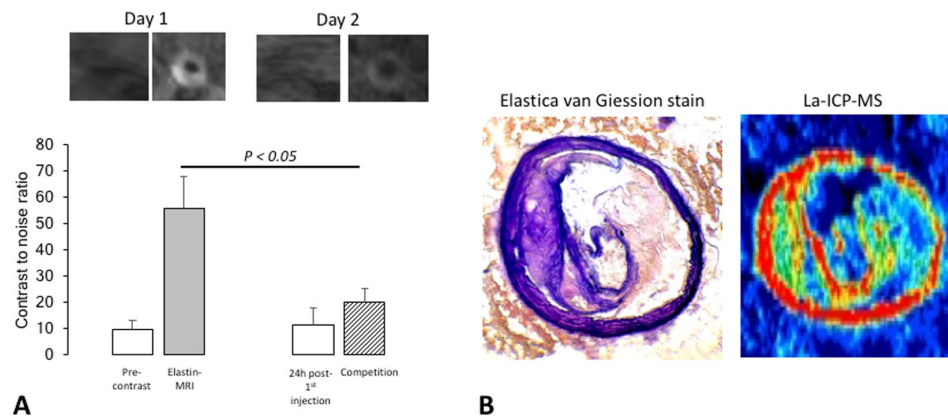


Figure 6. Competition experiments and laser ICP-MS for the mapping of the gadolinium distribution in an atherosclerotic-plaque. (A) First a pre-contrast scan was acquired on day one. In the next step 0.2 mmol/kg of the gadolinium-based elastin-specific probe was administered to assess the uptake of the probe in the vessel-wall. After 24-hours, a pre-contrast scan was repeated to confirm the washout of the agent. For the competition experiments, a tenfold-higher dose of non-paramagnetic europium-labeled elastin-specific MR-probe was administered prior to the application of 0.2 mmol/kg of the gadolinium-based elastin-specific probe. This resulted in a marked decrease of the contrast-to-noise-ratio compared to the administration of the gadolinium labeled elastin-specific agent alone. The *in vivo* competition experiments were performed in ApoE^{-/-} mice ($n = 3$) on a four-months high-fat-diet. (B) Spatial localization of the gadolinium-based elastin-specific probe using LA-ICP-MS. Signal from gadolinium across the arterial-wall sample ($n = 3$) was mapped to determine the distribution of gadolinium. Co-localization of targeted gadolinium with elastic-fibers was found.

www.nature.com/scientificreports/

macrophage-specific iron-oxide-based probe. Elastic-fibers play an important role during the pathogenesis of atherosclerosis¹⁵. Besides their elastic properties, elastic-fibers also have molecular signaling functions in atherosclerosis, influencing cell proliferation/migration and the retention of lipoproteins¹⁵.

Inflammation is considered to be a main drivers of atherosclerosis and especially macrophages are thought to play a central role¹⁶. Lipoproteins lead to a recruitment of monocytes/macrophages into the subendothelial space, where these cells phagocytose accumulating lipoproteins¹⁷.

The initiation and progression of atherosclerotic-plaques is a highly complex process, in which various cellular and matrix associated processes occur simultaneously. Different features that are associated with plaque vulnerability can be imaged based on the different available imaging techniques. In recent years, especially the visualization and quantification of vascular-remodeling and inflammation have been shown to represent promising biomarkers for improving the prediction of plaque vulnerability and the associated clinical events¹⁸.

Atherosclerosis associated vascular-remodeling is a process during which arteries enlarge to compensate for the development of the atherosclerotic-plaque. In the context of atherosclerosis, this process was first described and quantified by Glagov *et al.*⁵. The noninvasive quantification of vascular-remodeling was shown to be a highly promising biomarker to identify early subclinical disease, for the detection of unstable plaque and to monitor the progression and regression of atherosclerosis, e.g. in response-to-therapy. In this context, optical-coherence-tomography (OCT) and intravascular-ultrasound (IVUS) studies demonstrated that positive vascular-remodeling is a relevant feature of vulnerable atherosclerotic-plaques¹⁹. Previous studies have shown that the elastin-specific gadolinium-based probe used in the present study could be used to visualize elastin in the arterial-wall and that it may be used as a surrogate marker for plaque-burden and vascular-remodeling^{11,12}. Gadolinium-based probes are visualized as a result of the shortening of the T1-relaxation-times, resulting in a bright signal on T1-weighted images.

Various preclinical and clinical studies have investigated the use of iron-oxide-particles for the visualization of intraplaque macrophages²⁰. In the clinical setting, iron-oxide-particle accumulation in atherosclerotic-plaques correlated with the number of intraplaque macrophages²¹. It was also shown that ruptured or rupture prone plaques show a significantly higher accumulation of iron-oxide-particles compared to stable lesions. Regarding the assessment of response-to-therapy, the ATHEROMA study demonstrated, that the response to statin's anti-inflammatory effects could be assessed using iron-oxide-particles²². Iron-oxide-particles are visualized as a result of the shortening of the local T2/T2*-relaxation-times, creating a detectable signal-void on T2/T2*-weighted images.

For the visualization of the different probes, we used specific sequences. It however has to be considered that T1 and T2 probes also have minor effects on the T2 and T1 relaxation, especially if probes which exhibit a strong effect on both, T1 and T2 relaxation, are used.

This was also the first study, directly investigating the temporal association between intraplaque inflammation and extracellular-matrix remodeling in a single scan. In the current study, we could demonstrate that plaque inflammation and extracellular-matrix remodeling show a different temporal evolution during plaque development. In the early-phase, a pronounced accumulation of iron-oxide-particles was observed, which was in good agreement with a strong inflammatory process as shown by histology. In advanced plaques, a strong expression of elastic-fibers was observed. In response-to-therapy, a pronounced reduction in the accumulation of iron-oxide-particles was measured. These findings indicate that the development of atherosclerotic-plaque in this model is characterized by an early inflammation process, followed by cell migration and finally by extracellular-matrix remodeling (as typically seen in tissue injury such as myocardial infarction). There was no direct temporal association between extracellular-matrix remodeling and inflammation.

The use a two probes at the same time could be associated with challenges regarding a broad clinical translation. However, in the context of PET/MR imaging two probes (e.g. Gadovist and FDG) are also used in combination for tumor detection. The advantage of dual probe MR imaging would be the lack of ionizing radiation in this context.

An additional important finding of this study was that the gadolinium-based and iron-oxide-based probe used in these experiments do not affect the visualization and quantification of the respective other probe, which is especially relevant in a clinical setting.

Translational potential of this study. The gadolinium-based molecular probe used in this study was administered at a clinical dose and the molecular-weight and signal properties of the probe are comparable to currently used clinical contrast-agents. The applied iron-oxide-particle (also used at a clinical dose) is clinically approved and is currently successfully used as an imaging-agent in a clinical setting. Results from this study can be directly translated to human applications, using the same dose and with identical relaxation/rotational-correlation properties of the probes used.

Mouse-model used in this study. Previous studies have demonstrated that the brachiocephalic-artery of the ApoE^{-/-} mouse-model exhibits a consistent rate of lesion development/progression and that lesions show comparable features as observed during the different stages of plaque development in humans²³. A main limitation of animal models in general is, that they never fully resemble human disease.

Conclusion

This study demonstrates the feasibility of a simultaneous dual-probe molecular MRI for the simultaneous characterization of plaque-burden and inflammatory activity by in a mouse-model of progressive atherosclerosis. The *in-vivo* detection and quantification of these biomarkers associated with plaque instability in a single scan may enable the detection of potentially unstable plaque and thereby improve risk stratification and guidance of treatment and allow to monitor treatment response.

www.nature.com/scientificreports/

Data Availability

The datasets generated and analysed during the current study are available from the corresponding author on reasonable request.

References

- Rosamond, W. *et al.* Heart disease and stroke statistics—2007 update: a report from the American Heart Association Statistics Committee and Stroke Statistics Subcommittee. *Circulation* **115**, 69–6171 (2007).
- Libby, P. & Theroux, P. Pathophysiology of coronary artery disease. *Circulation* **111**, 3481–3488 (2005).
- Sato, Y., Hatakeyama, K., Marutsuka, K. & Asada, Y. Incidence of asymptomatic coronary thrombosis and plaque disruption: comparison of non-cardiac and cardiac deaths among autopsy cases. *Thromb Res* **124**, 19–23 (2009).
- Daemen, J. *et al.* Long-term safety and efficacy of percutaneous coronary intervention with stenting and coronary artery bypass surgery for multivessel coronary artery disease: a meta-analysis with 5-year patient-level data from the ARTS, ERACI-II, MASS-II, and SoS trials. *Circulation* **118**, 1146–1154 (2008).
- Glagov, S., Weisenberg, E., Zarins, C. K., Stankunavicius, R. & Kolettis, G. J. Compensatory enlargement of human atherosclerotic coronary arteries. *N Engl J Med* **316**, 1371–1375 (1987).
- Ambrose, J. A. *et al.* Angiographic progression of coronary artery disease and the development of myocardial infarction. *J Am Coll Cardiol* **12**, 56–62 (1988).
- Vancraeynest, D., Pasquet, A., Roelants, V., Gerber, B. L. & Vanoverschelde, J. L. Imaging the vulnerable plaque. *J Am Coll Cardiol* **57**, 1961–1979 (2011).
- Demeure, F. *et al.* Response by Demeure *et al.* to Letter Regarding Article, “Head-to-Head Comparison of Inflammation and Neovascularization in Human Carotid Plaques: Implications for the Imaging of Vulnerable Plaques”. *Circ Cardiovasc Imaging* **10** (2017).
- Di Corato, R. *et al.* High-resolution cellular MRI: gadolinium and iron oxide nanoparticles for in-depth dual-cell imaging of engineered tissue constructs. *ACS Nano* **7**, 7500–7512 (2013).
- Tyagi, P. *et al.* Novel contrast mixture improves bladder wall contrast for visualizing bladder injury. *Am J Physiol Renal Physiol* **313**, F155–F162 (2012).
- Makowski, M. R. *et al.* Assessment of atherosclerotic plaque burden with an elastin-specific magnetic resonance contrast agent. *Nat Med* **17**, 383–388 (2011).
- Onthank, D., Yalamanchili, P. & Cesati, R. & al, e. A novel low molecular weight magnetic resonance contrast agent selective for arterial wall imaging. *Circulation* **116**, II 411–II 412 (2007).
- Toth, G. B. *et al.* Current and potential imaging applications of ferumoxytol for magnetic resonance imaging. *Kidney Int* **92**, 47–66 (2017).
- Knobloch, G. *et al.* Relaxivity of Ferumoxytol at 1.5 T and 3.0 T. *Invest Radiol* **53**, 257–263 (2018).
- Katsuda, S. & Kaji, T. Atherosclerosis and extracellular matrix. *J Atheroscler Thromb* **10**, 267–274 (2003).
- Libby, P. Inflammation in atherosclerosis. *Nature* **420**, 868–874 (2002).
- Moore, K. J., Sheedy, F. J. & Fisher, E. A. Macrophages in atherosclerosis: a dynamic balance. *Nat Rev Immunol* **13**, 709–721 (2013).
- Saba, L. *et al.* Imaging biomarkers of vulnerable carotid plaques for stroke risk prediction and their potential clinical implications. *Lancet Neurol* **18**, 559–572 (2019).
- Ward, M. R., Pasterkamp, G., Yeung, A. C. & Borst, C. Arterial remodeling. Mechanisms and clinical implications. *Circulation* **102**, 1186–1191 (2000).
- Hyafil, F. *et al.* Ferumoxtran-10-enhanced MRI of the hypercholesterolemic rabbit aorta: relationship between signal loss and macrophage infiltration. *Arterioscler Thromb Vasc Biol* **26**, 176–181 (2006).
- Trivedi, R. A. *et al.* Identifying inflamed carotid plaques using *in vivo* USPIO-enhanced MR imaging to label plaque macrophages. *Arterioscler Thromb Vasc Biol* **26**, 1601–1606 (2006).
- Tang, T. Y. *et al.* The ATHEROMA (Atorvastatin Therapy: Effects on Reduction of Macrophage Activity) Study. Evaluation using ultrasmall superparamagnetic iron oxide-enhanced magnetic resonance imaging in carotid disease. *J Am Coll Cardiol* **53**, 2039–2050 (2009).
- Johnson, J. *et al.* Plaque rupture after short periods of fat feeding in the apolipoprotein E-knockout mouse: model characterization and effects of pravastatin treatment. *Circulation* **111**, 1422–1430 (2005).

Acknowledgements

This study was funded by the Deutsche Forschungsgemeinschaft (DFG, German Research Foundation) – SFB 1340/1 2018 and MA 5943/3-1/4-1/9-1 and the British Heart Foundation (BHF) RG/12/1/29262. The elastin-agent was provided by Lantheus Medical Imaging, North Billerica, Massachusetts, USA. The authors are thankful for performed ICP-MS by A.C., Mass-Spectrometry-Facility, King's College London and LA-ICP-MS by A.K. und U.S., Forschungszentrum Jülich, Germany. L.A. is grateful for her participation in the BIH-Charité-Junior Clinician-Scientist-Program funded by the Charité – Universitätsmedizin-Berlin and the Berlin-Institute-of-Health. The authors declare, that there is no conflict of interest regarding the publication of this article.

Author Contributions

Conception and design of the manuscript and analysis and interpretation of data: Marcus Makowski, Carolin Reimann. Drafting o the manuscript: Marcus Makowski, Carolin Reimann, Lisa C. Adams. Final approval of the manuscript: Julia Brangschi, Jan O. Kaufmann, Lisa C. Adams, David C. Onthank, Christa Thöne-Reineke, Simon P. Robinson, Bernd Hamm, Rene M. Botnar

Additional Information

Supplementary information accompanies this paper at <https://doi.org/10.1038/s41598-019-50100-8>.

Competing Interests: The authors declare no competing interests.

Publisher's note Springer Nature remains neutral with regard to jurisdictional claims in published maps and institutional affiliations.

www.nature.com/scientificreports/



Open Access This article is licensed under a Creative Commons Attribution 4.0 International License, which permits use, sharing, adaptation, distribution and reproduction in any medium or format, as long as you give appropriate credit to the original author(s) and the source, provide a link to the Creative Commons license, and indicate if changes were made. The images or other third party material in this article are included in the article's Creative Commons license, unless indicated otherwise in a credit line to the material. If material is not included in the article's Creative Commons license and your intended use is not permitted by statutory regulation or exceeds the permitted use, you will need to obtain permission directly from the copyright holder. To view a copy of this license, visit <http://creativecommons.org/licenses/by/4.0/>.

© The Author(s) 2019

Supplementary material

Materials and Methods

Animals

Mice were housed under controlled conditions (12:12 h light/dark cycle, lights on 07:00 h, temperature, 22 ± 2 °C) and provided with food and water *ad libitum*. Eight weeks old homozygous apolipoprotein E-deficient (ApoE-/-) male mice were used (Forschungseinrichtung für experimentelle Medizin (FEM), Berlin, Germany). For imaging controls, nine 26 week old male homozygous C57BL/6J mice from Charles River Laboratories (Sulzfeld, Germany) were used.

All animals were housed in a clean barrier. Prior to imaging sessions, mice were anesthetized using an intraperitoneal administration of a combination of Medetomidin (500 µg/kg), Fentanyl (50 µg/kg) and Midazolam (5 mg/kg). For serial imaging experiments, a reversal agent, consisting of Atipamezol (2.5 mg/kg), Flumazenil (500 µg/kg) and Naloxon (1200 µg/kg), was administered after the imaging session [68]. Following the final imaging session, mice were euthanized. For histological examinations, a perfusion with the fixative MorFFFix® (Morphisto, Frankfurt am Main, Germany) at a pressure of 100 mm Hg was performed followed by excision of the carotid arteries, brachiocephalic artery and aortic artery. All animal procedures were carried out by a veterinarian and all possible steps were taken to avoid animal suffering at all time points of the experiments.

In Vivo MR Experiments

For the administration of the different MR imaging-agents, a small diameter tube with an attached needle was inserted into the tail vein of the animals. During the imaging sessions, body temperature (37 °C) was monitored using a MR-compatible heating system (Model 1025, SA Instruments Inc, Stony Brook, NY).

Elastin imaging using T1-weighted sequences

For localization of the aortic artery, brachiocephalic artery and carotid arteries, a low-resolution three-dimensional (3D) localizer scan was performed in sagittal, coronal and transverse orientation using the following parameters: field-of-view (FOV) = 280 mm, matrix = 320, slice thickness = 3 mm, TR/TE = 7.7/3.7 ms, flip angle = 20° and slices = 10. The scout scan was

followed by a two-dimensional (2D) time-of-flight (TOF) scan in transverse orientation for visualization of the aortic arch and the brachiocephalic artery. Imaging parameters included: FOV = 200 mm, matrix = 960, in plane spatial resolution = 0.2 x 0.2 mm, slice thickness = 500 μ m, TR/TE = 35/4.5 ms, flip angle = 90° and slices = 26. From the TOF dataset, a maximum intensity projection (MIP) was generated for display of an arterial angiogram of the aortic arch, the brachiocephalic artery and the carotid arteries to plan the subsequent contrast-enhanced sequences. The inversion recovery scan to visualize the gadolinium-based contrast agent was preceded by a 2D Look-Locker sequence planned perpendicular to the ascending aorta, which was used to determine the optimal inversion time (TI) for blood signal nulling. Imaging parameters of the Lock Locker sequence included: FOV = 300 mm, matrix = 750, in plane spatial resolution = 0.4 x 0.4 mm, slice thickness = 1.5 mm, TR between subsequent IR pulses = 1000 ms, and flip angle = 15°. Imaging parameters of the high-resolution 3D inversion recovery gradient echo late gadolinium enhancement (LGE) sequence scan employed for visualization of gadolinium-based molecular probe were: FOV = 57 mm, matrix = 416, inplane spatial resolution = 0.137 x 0.137 mm, slice thickness = 370 μ m, slices = 56, TR/TE = 12.1/5.7 ms, TR between subsequent IR pulses = 1000 ms, and flip angle = 30°.

Iron oxide imaging using T2-weighted sequences*

Imaging parameters for the T2* weighted sequences in this study included a field of view 150 x 150 mm; matrix 832 x 832; in-plane spatial resolution 0.18 x 0.18 mm; slice thickness 500 μ m; TR/TE 17/7.4 ms; flip angle 20°; averages, Phase Partial Fourier 6/8, and 32 slices.

Histological analysis and immunofluorescence of the arterial vessel system and plaque morphometry

Histological analysis of the brachiocephalic artery was performed as described below. The vessels were embedded in paraffin and cut into 5 μ m thick serial sections. These sections were dewaxed and stained with Miller's Elastica-van-Gieson-stain (EvG) for visualization of elastin and Perls' Prussian-blue-stain for the visualization of iron-oxide-particles. Additionally, a standard Hematoxylin-and-Eosin (HE) stain was performed. For co-registration of histological sections and MR images, the aortic arch and the subclavian artery were used as landmarks. Analyses were made on digitized images of EvG, Perls' Prussian blue and immunofluorescence sections. Morphometry as well as quantification of staining area were

measured using computer-assisted image-analysis (ImageJ software, Version 1.51). Immunofluorescence staining of macrophages using a primary antibody (rat anti mouse CD68, Bio-Rad, 1:100) and Dako REALTM Antibody Diluent (Dako, Denmark) required incubation overnight at 8 degrees. Sections were washed two times with PBS, pH 7.4. Macrophages binding was located by incubation with the polyclonal secondary Antibody (goat anti-rat IgG, Thermo Fisher Scientific, Germany, 1:200). Slides were washed three times with PBS, pH 7.4, counterstained and mounted with Roti[®]-Mount FlourCare (Carl Roth, Germany). Co-registration of macrophages on CD68 staining and Perls' Prussian blue positive staining areas was assessed in serial sections of atherosclerotic lesions.

Inductively coupled mass spectrometry for quantification of gadolinium and iron and Laser-inductively-coupled-mass-spectrometry (LA ICP-MS) for spatial localization of gadolinium

Inductively coupled mass spectrometry (ICP-MS) was conducted using vessel tissue samples at each time point (n=3 per group). After the last imaging session, brachiocephalic samples were digested at 37°C in 70% nitric acid overnight, followed by dilution with deionized water to an acid concentration of 2.5% for ICP-MS analysis. For each sample set a standard curve was documented for iron oxide and gadolinium concentration.

Brachiocephalic arteries were cut at -20 °C into 10 µm cryosections and immediately mounted on SuperFrost Plus adhesion slides (Thermo Scientific). The laser ablation was performed with a laser ablation system NWR 213 (New Wave Research, Fremont, CA, USA) connected to an inductively coupled plasma mass spectrometer (Agilent 7900, Agilent Technologies, Japan) using line scans with a laser energy of 34%, a spot size of 20 µm and a measurement speed of 20 µm/s. For quantification of the Gadolinium (Gd) amount in brachiocephalic arteries, rat brain standards with well-defined Gd concentration were analyzed under the same conditions. The calibration, the reconstruction, and the visualization of the images were performed by an in-house developed software (ForschungszentrumJülich, Jülich, Germany).Methods were established as mentioned in our previous studies (Supplementary References 1-3).

Competition experiments

In vivo competition experiments were performed in ApoE-/- mice ($n = 3$) on a four months high-fat-diet. The elastin-specific probe, ESMA, was administered on day one at a clinically relevant dose of 0.2 mmol/kg. After the day one scanning session, a preinjection of a tenfold higher dose of the non-paramagnetic europium-labeled elastin-specific MR probe was performed. On day two, the elastin-specific probe was administered at a clinically relevant dose of 0.2 mmol/kg. All contrast agents were applied *via* the tail vein.

Statistical Analysis

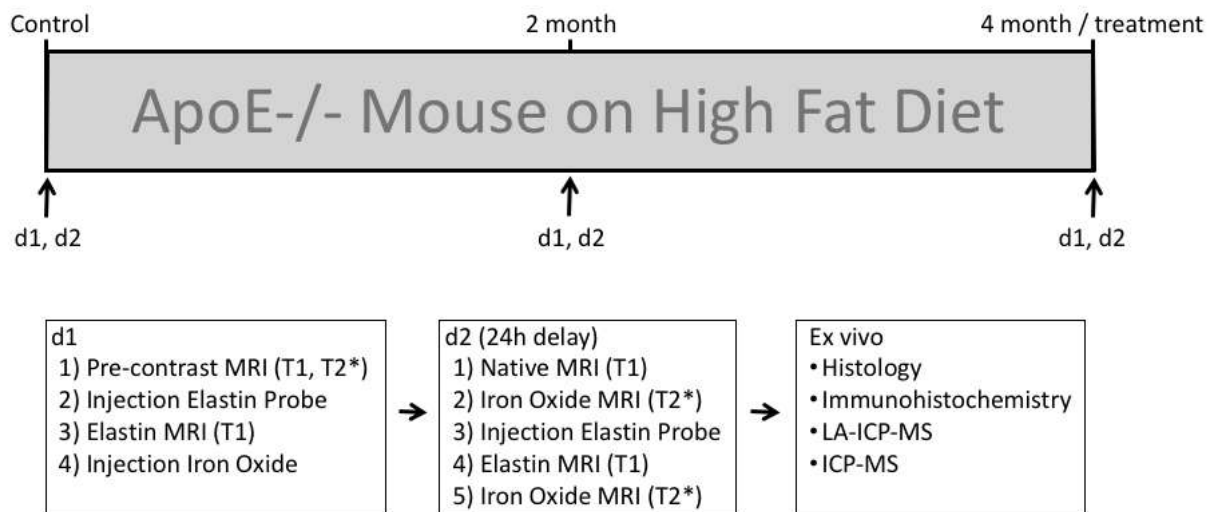
Values are specified as mean \pm standard deviation. Values of the treatment and control group were compared using SigmaStat 4.0 (Systat Software, Inc). For the comparison of continuous variables, a Student's t test (unpaired, two-tailed) was applied. In case of more than two groups, statistical comparisons were performed by analysis of variance (ANOVA) followed by the Bonferroni test. $p < 0.05$ was regarded to be statistically significant.

Supplementary References:

1. Makowski MR, Wiethoff AJ, Blume U, Cuello F, Warley A, Jansen CH, et al. Assessment of atherosclerotic plaque burden with an elastin-specific magnetic resonance contrast agent. *Nat Med.* 2011;17(3):383-8.
2. Makowski MR, Preissel A, von Bary C, Warley A, Schachoff S, Keithan A, et al. Three-dimensional imaging of the aortic vessel wall using an elastin-specific magnetic resonance contrast agent. *Invest Radiol.* 2012;47(7):438-44.
3. Reimann C, Brangsch J, Kaufmann JO, Adams LC, Onthank DC, Robinson SP, et al. Contrast-Enhanced Magnetic Resonance Angiography Using a Novel Elastin-Specific Molecular Probe in an Experimental Animal Model. *Contrast Media Mol Imaging.* 2018;2018:9217456

Supplementary Figure 1: Experimental setup of the study.

The animal was imaged at two time points, on day one and after 24 hours on day two. On day one, first a pre-contrast MRI with a T1 and T2*-weighted sequence was performed. Then the elastin-specific probe was injected at the clinical dose of 0.2 mmol/kg. After 40 minutes the T1-weighted MR sequences were performed. After the imaging session was finished, the iron oxide particle (ferumoxytol) was injected at a clinical dose of 4mg Fe/kg. On day two, first a native T1-weighted MR sequence was performed to exclude any residual binding of the elastin agent in the vessel wall. Then the T2*-weighted sequence was acquired to measure the accumulation of the iron oxide particles in the vascular wall. Following that the elastin-specific probe was injected for a second time. After 40 minutes, a T1-weighted MR sequence was performed to assess the uptake of the probe in the vessel wall. Following this, an additional T2*-weighted sequence was performed to exclude any effect of the gadolinium-based probe on the T2* images. Following the final imaging session, the brachiocephalic artery was surgically removed for further *ex vivo* analysis.

Supplementary Figure 1

3. Diskussion

Zur Darstellung des Gefäßsystems bei Patienten und zur Charakterisierung von Gefäßwandpathologien wie Atherosklerose werden verschiedene Arten von MR-Kontrastmittel benutzt, darunter Kontrastmittel auf Gadolinium- und Eisenoxidbasis [69, 70]. Als Teil dieser Arbeit wurde eine neuartige molekulare elastinspezifische Sonde auf Gadoliniumbasis mit dem klinischen Kontrastmittel Gadobutrol für die Durchführung einer MR-Angiographie verglichen. In der klinischen Praxis werden am häufigsten MRT-Kontrastmittel auf der Basis von Gadoliniumchelaten verwendet. Die wichtigste klinische Anwendung dieser MRT-Kontrastmittel ist die Visualisierung der verschiedenen Gefäßstrukturen. Aus den unterschiedlichen MRT-Signalen werden wichtige klinische Informationen zur Charakterisierung von Pathologien abgeleitet. Wenn eine neuartige Sonde in die klinische Praxis eingeführt wird, sollte die Sonde idealerweise, neben ihren molekularen Eigenschaften, auch die Visualisierung der verschiedenen Blutgefäßphasen (arteriellen, venösen und verzögerte Phase) ermöglichen. Die aktuell klinisch verwendeten MR-Kontrastmittel verteilen sich nach der intravenösen Injektion und der frühen Blutphase schnell aus dem arteriellen und venösen Lumen in den extrazellulären Raum, das bedeutet, dass Gefäßwandpathologien wie Atherosklerose schwieriger darzustellen sind. In der ersten Arbeit dieser Dissertation haben wir die Eigenschaften einer neuartigen elastinspezifischen molekularen Sonde auf Gadoliniumbasis zur Visualisierung der klinisch wichtigen frühen arteriellen Phasen dieses Kontrastmittels untersucht. Wichtig ist, dass alle Messungen mit derselben klinisch relevanten Dosis (0,1 mmol / kg) und mit einer einzigen Bolusgabe durchgeführt wurden, um beide Kontrastmittel genau miteinander vergleichen zu können. Die paramagnetische Gadolinium-markierte elastinspezifische molekulare Sonde ist eine Sonde mit niedrigem Molekulargewicht (856 Dalton). Vergleichbar mit klinisch verwendeten Kontrastmitteln auf Gadoliniumbasis ist diese Sonde mit einem Gadoliniumchelat markiert [20]. Aufgrund ihrer geringen Größe zeigt diese Sonde eine schnelle Clearance aus dem Blutpool. Es konnte gezeigt werden, dass die Bildgebungseigenschaften der molekularen elastinspezifischen Sonde vergleichbar zu den routinemäßig verwendeten klinischen Kontrastmitteln wie Gadobutrol für die Durchführung einer MR-Angiographie sind. Die Bildgebung wurde analog zur klinischen Praxis in Bezug auf die verwendeten MR-Sequenzen, die Feldstärke von 3 Tesla und das MRT-Gerät durchgeführt. Die Darstellung mittels MR-Angiographie ist sehr detailgetreu und ermöglicht die 3D-Rekonstruktion zur genauen Darstellung sowie Therapieplanung. Nach der intravenösen Injektion zeigten beide Sonden eine schnelle renale Clearance aus dem Blutpool. Aufgrund dieser Eigenschaft konnte das höchste intravaskuläre MRT-Signal während der ersten Phase nach der

intravenösen Verabreichung erreicht werden. Diese *in vivo* Studie untermauert die Ergebnisse früherer Studien [20, 71-73]. Die Signalverstärkung der Gefäße durch das elastinspezifische Kontrastmittel war vergleichbar zu der Messung mit dem klinisch verwendeten Kontrastmittel (Gadobutrol). In Bezug auf die Umsetzung in klinische Anwendungen bietet die neuartige molekulare elastinspezifische Sonde mehrere Vorteile. Die gesamte Bildgebung wurde mit einem klinischen 3T-MRT-System durchgeführt. Daher bleiben die Signaleigenschaften des Kontrastmittels unverändert, und die Bildgebungseigenschaften können daher direkt auf die Anwendung am Menschen übertragen werden. Die molekulare Zusammensetzung und Größe des Kontrastmittels ist vergleichbar mit den bereits in der klinischen Praxis verwendeten Kontrastmitteln, so dass unerwünschte Wirkungen im Vergleich zu größeren Molekülen wesentlich unwahrscheinlicher sind.

Zusammenfassend zeigt diese erste Arbeit, dass die elastinspezifische molekulare Sonde klinisch nutzbare Signaleigenschaften für die Erfassung von zeitaufgelöster First-Pass-Magnetresonanz-Angiographie (MRA) und späten 3D-MR-Angiographien aufweist.

Im zweiten Teil dieser Dissertation wird die Durchführbarkeit einer Multisonden-MRT zur simultanen Charakterisierung des Remodeling der extrazellulären Matrix und der entzündlichen Aktivität für progressive Atherosklerose untersucht. Atherosklerose-assoziiertes Gefäß-Remodelling ist ein Prozess, bei dem sich die Arterien im Umfang vergrößern. Im Zusammenhang mit Atherosklerose wurde dieser Prozess zuerst von Glagov et al. [39] nachgewiesen. Gefäßstenosen können dabei langsam fortschreiten. Die Plaques, welche die stenotischen Bereiche verursachen, neigen dazu, trotz erhöhter Strömungsgeschwindigkeiten des Blutes bei diesen Verengungen stabil zu bleiben. Die meisten schwerwiegenden Ereignisse treten bei großen Plaques auf, die vor ihrem Aufbrechen sehr wenig oder gar keine Stenose hervorriefen. Aus klinischen Studien geht hervor, dass 20% der durchschnittliche Stenosegrad ist, bei dem die Plaques brechen und abschwemmen und anschließend einen vollständigen Verschluss der Arterie zur Folge haben. Glagov et al. [39] zeigte, dass die nichtinvasive Quantifizierung des Gefäßdurchmessers ein vielversprechender Biomarker ist, um eine frühe subklinische Erkrankung zu identifizieren, instabile Plaque zu erkennen und das Fortschreiten und die Rückbildung von Atherosklerose zu überwachen. Die Entstehung und das Fortschreiten von atherosklerotischen Plaques ist ein hochkomplexer Prozess, bei dem verschiedene zelluläre und matrixassoziierte Prozesse zum Teil simultanen und zum Teil subsequent ablaufen. Dabei spielen elastische Fasern eine wichtige Rolle besonders beim Fortschreiten der

Atherosklerose [21]. Die Entzündung der Gefäßwand gilt als eine wichtige Komponente bei der Initiierung der Atherosklerose, wobei insbesondere Makrophagen eine zentrale Rolle spielen [9]. Auf der Grundlage der verfügbaren Bildgebungstechniken können verschiedene Merkmale abgebildet werden, die mit den Plaques verbunden sind. Die gegenwärtig klinisch verwendeten MR-Kontrastmittel sammeln sich in Bereichen mit fibrotischem Gewebe an. Da es sich jedoch um einen „passiven“ Prozess handelt, der nicht gegen ein bestimmtes Protein oder eine bestimmte Zelle gerichtet ist, liefern sie nur indirekte / unspezifische und begrenzte Informationen über pathologische Prozesse. In den letzten Jahren hat sich gezeigt, dass insbesondere die Visualisierung und Quantifizierung des Gefäßumbaus sowie der Entzündungsaktivität vielversprechende Biomarker zur Verbesserung der Vorhersage der Plaqueruptur und der damit verbundenen klinischen Ereignisse darstellen [74]. In diesem Teil der Dissertation wurden zwei verschiedene molekulare Biomarker, eine elastinspezifische Sonde auf Gadoliniumbasis und eine makrophagenspezifische Sonde auf Eisenoxidbasis, simultan *in vivo* eingesetzt und untersucht. Mit Hilfe dieser molekularen Sonden konnte erstmals eine zeitliche Verzögerung zwischen der De-novo-Synthese von elastischen Fasern und der entzündlichen Aktivität in atherosklerotischen Plaques visualisiert werden. Während die Entzündung in frühen atherosklerotischen Plaques ausgeprägter war und diese ein stärkeres Ansprechen auf die Statintherapie zeigte, war die Elastinexpression in fortgeschrittenen atherosklerotischen Plaques am ausgeprägtesten. In dieser Arbeit wurde die erste *in vivo* MR-Studie durchgeführt, welche zeigte, dass sowohl der strukturelle Umbau der extrazellulären Matrix als auch die Entzündung mit Hilfe eines Multisonden-Ansatzes in einer einzelnen MR-Untersuchung quantifiziert werden kann. Darüber hinaus wurde gezeigt, dass sich die Sonden auf Gadolinium- und Eisenoxidbasis nicht gegenseitig beeinflussen und die Quantifizierung der jeweiligen Zielstrukturen nicht beeinträchtigt wurde. In dieser Studie stimmte die *in vivo*-Plaquebelastungsmessung, die mittels MR-Bildgebung bewertet wurden, mit der *ex vivo*-Plaquebelastungsmessung der histopathologischen Untersuchung überein. Der gleichzeitige *in vivo* Nachweis und die Quantifizierung von Entzündungen und strukturellen Umbau der extrazellulären Matrix könnten für eine verbesserte Charakterisierung und Darstellung von atherosklerotischen Läsionen, einschließlich der Bewertung des Ansprechens auf Therapie, nützlich sein.

Dies war die erste Studie, welche den zeitlichen Zusammenhang zwischen der Entzündungsaktivität und extrazellulärem Matrixumbau in einem simultanen Scan untersuchte. Die niedermolekularen Sonden sind somit für die Charakterisierung von Gefäßerkrankungen mittels MRT geeignet.

4. Zusammenfassung „Entwicklung und Evaluierung neuer niedrig-molekularer Sonden für die Charakterisierung von Gefäßerkrankungen mittels der Magnetresonanztomographie (MRT)“

Atherosklerose ist von fundamentaler Bedeutung für zahlreiche kardiovaskulärer Folgeerkrankungen. Klinisch äußert sie sich meist erst nach Jahren oder Jahrzehnten durch Symptome ihrer Folgeerkrankungen. Die zentralen pathophysiologischen Faktoren dieser Erkrankung sind Endothelzelldysfunktionen, Ablagerungen von Blutfetten in den Gefäßwänden und chronische Entzündungsreaktionen. Kennzeichnend für Atherosklerose ist also die Ansammlung von proinflammatorischen Zellen und extrazellulären Matrixproteinen, wie Elastin, in der Gefäßintima. Ein Risiko für Atherosklerose ist die Plaqueruptur mit der subsequenten Bildung von Thromben, welche zu Herzinfarkten oder Schlaganfällen führen können. Präventionsansätze können die Mortalität dieser Krankheit drastisch senken. Die molekulare Bildgebung ermöglicht die nicht-invasive *in vivo* Visualisierung und Quantifizierung biologischer Prozesse auf molekularer und zellulärer Ebene. Diese Dissertation hat sich mit dem Potenzial der *in vivo* Magnetresonanztomographie für die molekulare Bildgebung von Atherosklerose befasst und neue Möglichkeiten in der Detektion dieser Erkrankung aufgezeigt.

Zum einen wurde im ersten Teil dieser Dissertation gezeigt, dass die elastinspezifische Sonde ähnliche Eigenschaften für die Durchführung von MR-Angiographien hat, wie klinisch verwendete Kontrastmittel. Dies ist von hoher Relevanz für die potentielle klinische Translation einer solchen Sonde.

Zum anderen konnte im zweiten Teil dieser Dissertation gezeigt werden, dass auf Basis einer simultanen molekularen MRT mit zwei Sonden die Charakterisierung der Plaquelast und der entzündlichen Aktivität von progressiver Atherosklerose im Mausmodell möglich ist. Der *in vivo* Nachweis und die Quantifizierung dieser mit Plaque-Instabilität verbundenen Biomarker in einem einzigen Scan können den Nachweis von instabilen Plaques ermöglichen und dadurch die Risikostratifizierung und Behandlungsführung von Patienten verbessern. Die duale Anwendung der elastin- und eisenoxidspezifischen Sonden bildet somit ein neuartiges BildgebungsInstrument zur *in vivo* Charakterisierung der Plaqueruptur bei Atherosklerose.

5. Summary „Development and Evaluation of new low-molecular probes for the characterization of vascular diseases by magnetic resonance imaging (MRI)“

Atherosclerosis is of fundamental importance for numerous cardiovascular sequelae. Clinically, it usually manifests itself only after years or decades by symptoms of their sequelae. The central pathophysiological factors of this disease are endothelial cell dysfunction, deposits of blood lipids in the vessel walls and chronic inflammatory reactions. Characteristic of atherosclerosis is therefore the accumulation of proinflammatory cells and extracellular matrix proteins, such as elastin, in the vascular intima. A risk of atherosclerosis is plaque rupture with the subsequent formation of thrombi, which can lead to heart attacks or strokes. Prevention approaches can drastically reduce the mortality of this disease. Molecular imaging enables the non-invasive *in vivo* visualization and quantification of biological processes at the molecular and cellular level. This dissertation deals with the potential of *in vivo* magnetic resonance tomography for the molecular imaging of atherosclerosis and demonstrates new possibilities in the detection of this disease.

On the one hand, the first part of this thesis demonstrated that the elastin-specific probe has similar properties for performing MR angiography as clinically used contrast agents. This is of high relevance for the potential clinical translation of such a probe.

On the other hand, in the second part of this thesis it could be shown that a simultaneous molecular MRI with two probes enables the characterization of the plaque burden and the inflammatory activity of progressive atherosclerosis in a mouse model. The *in vivo* detection and quantification of these plaque instability-associated biomarkers in a single scan can enable detection of unstable plaques, thereby improving patient risk stratification and treatment guidance. The dual application of the elastin and iron oxide specific probes thus forms a novel imaging instrument for the *in vivo* characterization of plaque rupture in atherosclerosis.

6. Literaturverzeichnis der Einleitung und Diskussion

1. Hartvigsen K, Chou MY, Hansen LF, Shaw PX, Tsimikas S, Binder CJ, Witztum JL. The role of innate immunity in atherogenesis. *J Lipid Res.* 2009;50 Suppl:S388-93.
2. Rosamond W, Flegal K, Friday G, Furie K, Go A, Greenlund K, Haase N, Ho M, Howard V, Kissela B, Kittner S, Lloyd-Jones D, McDermott M, Meigs J, Moy C, Nichol G, O'Donnell CJ, Roger V, Rumsfeld J, et al. Heart disease and stroke statistics--2007 update: a report from the American Heart Association Statistics Committee and Stroke Statistics Subcommittee. *Circulation.* 2007;115(5):e69-171.
3. Go AS, Mozaffarian D, Roger VL, Benjamin EJ, Berry JD, Borden WB, Bravata DM, Dai S, Ford ES, Fox CS, Franco S, Fullerton HJ, Gillespie C, Hailpern SM, Heit JA, Howard VJ, Huffman MD, Kissela BM, Kittner SJ, et al. Heart disease and stroke statistics--2013 update: a report from the American Heart Association. *Circulation.* 2013;127(1):e6-e245.
4. Yusuf S, Reddy S, Ounpuu S, Anand S. Global burden of cardiovascular diseases - Part I: General considerations, the epidemiologic transition, risk factors, and impact of urbanization. *Circulation.* 2001;104(22):2746-53.
5. Fuster V, Kelly B. Summary of the institute of medicine report promoting cardiovascular health in the developing world. *Glob Heart.* 2011;6(4):133-42.
6. Glass CK, Witztum JL. Atherosclerosis. the road ahead. *Cell.* 2001;104(4):503-16.
7. Lusis AJ. Atherosclerosis. *Nature.* 2000;407(6801):233-41.
8. Libby P. The molecular mechanisms of the thrombotic complications of atherosclerosis. *J Intern Med.* 2008;263(5):517-27.
9. Libby P. Inflammation in atherosclerosis. *Nature.* 2002;420(6917):868-74.
10. Libby P, Theroux P. Pathophysiology of coronary artery disease. *Circulation.* 2005;111(25):3481-8.
11. Sato Y, Hatakeyama K, Marutsuka K, Asada Y. Incidence of asymptomatic coronary thrombosis and plaque disruption: comparison of non-cardiac and cardiac deaths among autopsy cases. *Thromb Res.* 2009;124(1):19-23.
12. Sitia S, Tomasoni L, Atzeni F, Ambrosio G, Cordiano C, Catapano A, Tramontana S, Perticone F, Naccarato P, Camici P, Picano E, Cortigiani L, Bevilacqua M, Milazzo L, Cusi D, Barlassina C, Sarzi-Puttini P, Turiel M. From endothelial dysfunction to atherosclerosis. *Autoimmun Rev.* 2010;9(12):830-4.
13. Krettek A, Sukhova GK, Libby P. Elastogenesis in human arterial disease: a role for macrophages in disordered elastin synthesis. *Arterioscler Thromb Vasc Biol.* 2003;23(4):582-7.
14. Rouis M. Matrix metalloproteinases: a potential therapeutic target in atherosclerosis. *Curr Drug Targets Cardiovasc Haematol Disord.* 2005;5(6):541-8.
15. Henney AM, Wakeley PR, Davies MJ, Foster K, Hembry R, Murphy G, Humphries S. Localization of stromelysin gene expression in atherosclerotic plaques by in situ hybridization. *Proc Natl Acad Sci U S A.* 1991;88(18):8154-8.
16. Sukhova GK, Shi GP, Simon DI, Chapman HA, Libby P. Expression of the elastolytic cathepsins S and K in human atheroma and regulation of their production in smooth muscle cells. *J Clin Invest.* 1998;102(3):576-83.
17. Chatzizisis YS, Jonas M, Coskun AU, Beigel R, Stone BV, Maynard C, Gerrity RG, Daley W, Rogers C, Edelman ER, Feldman CL, Stone PH. Prediction of the localization of high-risk coronary atherosclerotic plaques on the basis of low endothelial shear stress: an intravascular ultrasound and histopathology natural history study. *Circulation.* 2008;117(8):993-1002.
18. Brasselet C, Durand E, Addad F, Al Haj Zen A, Smeets MB, Laurent-Maquin D, Bouthors S, Bellon G, de Kleijn D, Godeau G, Garnotel R, Gogly B, Lafont A. Collagen and elastin cross-linking: a mechanism of constrictive remodeling after arterial injury. *Am J Physiol Heart Circ Physiol.* 2005;289(5):H2228-33.

19. Woodley DT, Yamauchi M, Wynn KC, Mechanic G, Briggaman RA. Collagen Telopeptides (Cross-Linking Sites) Play a Role in Collagen Gel Lattice Contraction. *J Invest Dermatol.* 1991;97(3):580-5.
20. Makowski MR, Wiethoff AJ, Blume U, Cuello F, Warley A, Jansen CH, Nagel E, Razavi R, Onthank DC, Cesati RR, Marber MS, Schaeffter T, Smith A, Robinson SP, Botnar RM. Assessment of atherosclerotic plaque burden with an elastin-specific magnetic resonance contrast agent. *Nat Med.* 2011;17(3):383-8.
21. Katsuda S, Kaji T. Atherosclerosis and extracellular matrix. *J Atheroscler Thromb.* 2003;10(5):267-74.
22. Nili N, Zhang M, Strauss BH, Bendeck MP. Biochemical analysis of collagen and elastin synthesis in the balloon injured rat carotid artery. *Cardiovasc Pathol.* 2002;11(5):272-6.
23. Li DY, Brooke B, Davis EC, Mecham RP, Sorensen LK, Boak BB, Eichwald E, Keating MT. Elastin is an essential determinant of arterial morphogenesis. *Nature.* 1998;393(6682):276-80.
24. Isik FF, Clowes AW, Gordon D. Elastin expression in a model of acute arterial graft rejection. *Transplantation.* 1994;58(11):1246-51.
25. Nikkari ST, Jarvelainen HT, Wight TN, Ferguson M, Clowes AW. Smooth muscle cell expression of extracellular matrix genes after arterial injury. *Am J Pathol.* 1994;144(6):1348-56.
26. Masuda H, Zhuang YJ, Singh TM, Kawamura K, Murakami M, Zarins CK, Glagov S. Adaptive remodeling of internal elastic lamina and endothelial lining during flow-induced arterial enlargement. *Arterioscler Thromb Vasc Biol.* 1999;19(10):2298-307.
27. Matrisian LM. The matrix-degrading metalloproteinases. *Bioessays.* 1992;14(7):455-63.
28. Allaire E, Muscatelli-Groux B, Mandet C, Guinault AM, Bruneval P, Desgranges P, Clowes A, Melliere D, Becquemin JP. Paracrine effect of vascular smooth muscle cells in the prevention of aortic aneurysm formation. *J Vasc Surg.* 2002;36(5):1018-26.
29. Galis ZS, Khatri JJ. Matrix metalloproteinases in vascular remodeling and atherogenesis: the good, the bad, and the ugly. *Circ Res.* 2002;90(3):251-62.
30. Avolio A, Jones D, Tafazzoli-Shadpour M. Quantification of alterations in structure and function of elastin in the arterial media. *Hypertension.* 1998;32(1):170-5.
31. Zarins CK, Xu C, Glagov S. Atherosclerotic enlargement of the human abdominal aorta. *Atherosclerosis.* 2001;155(1):157-64.
32. Newby AC. Metalloproteinase expression in monocytes and macrophages and its relationship to atherosclerotic plaque instability. *Arterioscler Thromb Vasc Biol.* 2008;28(12):2108-14.
33. Streuli C. Extracellular matrix remodelling and cellular differentiation. *Curr Opin Cell Biol.* 1999;11(5):634-40.
34. Newby AC. Dual role of matrix metalloproteinases (matrixins) in intimal thickening and atherosclerotic plaque rupture. *Physiol Rev.* 2005;85(1):1-31.
35. Hopps E, Caimi G. Matrix metalloproteinases as a pharmacological target in cardiovascular diseases. *Eur Rev Med Pharmacol.* 2015;19(14):2583-9.
36. Raffetto JD, Khalil RA. Matrix metalloproteinases and their inhibitors in vascular remodeling and vascular disease. *Biochem Pharmacol.* 2008;75(2):346-59.
37. Williams H, Johnson JL, Carson KG, Jackson CL. Characteristics of intact and ruptured atherosclerotic plaques in brachiocephalic arteries of apolipoprotein E knockout mice. *Arterioscler Thromb Vasc Biol.* 2002;22(5):788-92.
38. Daemen J, Boersma E, Flather M, Booth J, Stables R, Rodriguez A, Rodriguez-Granillo G, Hueb WA, Lemos PA, Serruys PW. Long-term safety and efficacy of percutaneous coronary intervention with stenting and coronary artery bypass surgery for multivessel coronary artery disease: a meta-analysis with 5-year patient-level data from the ARTS, ERACI-II, MASS-II, and SoS trials. *Circulation.* 2008;118(11):1146-54.

39. Glagov S, Weisenberg E, Zarins CK, Stankunavicius R, Kolettis GJ. Compensatory enlargement of human atherosclerotic coronary arteries. *N Engl J Med.* 1987;316(22):1371-5.
40. Ambrose JA, Tannenbaum MA, Alexopoulos D, Hjemdahl-Monsen CE, Leavy J, Weiss M, Borrico S, Gorlin R, Fuster V. Angiographic progression of coronary artery disease and the development of myocardial infarction. *J Am Coll Cardiol.* 1988;12(1):56-62.
41. Vancraeynest D, Pasquet A, Roelants V, Gerber BL, Vanoverschelde JL. Imaging the vulnerable plaque. *J Am Coll Cardiol.* 2011;57(20):1961-79.
42. Massoud TF, Gambhir SS. Molecular imaging in living subjects: seeing fundamental biological processes in a new light. *Genes Dev.* 2003;17(5):545-80.
43. Flacke S, Fischer S, Scott MJ, Fuhrhop RJ, Allen JS, McLean M, Winter P, Sicard GA, Gaffney PJ, Wickline SA, Lanza GM. Novel MRI contrast agent for molecular imaging of fibrin: implications for detecting vulnerable plaques. *Circulation.* 2001;104(11):1280-5.
44. Klibanov AL, Rychak JJ, Yang WC, Alikhani S, Li B, Acton S, Lindner JR, Ley K, Kaul S. Targeted ultrasound contrast agent for molecular imaging of inflammation in high-shear flow. *Contrast Media Mol Imaging.* 2006;1(6):259-66.
45. Jaffer FA, Weissleder R. Molecular imaging in the clinical arena. *Jama-J Am Med Assoc.* 2005;293(7):855-62.
46. Nguyen QT, Olson ES, Aguilera TA, Jiang T, Scadeng M, Ellies LG, Tsien RY. Surgery with molecular fluorescence imaging using activatable cell-penetrating peptides decreases residual cancer and improves survival. *Proc Natl Acad Sci U S A.* 2010;107(9):4317-22.
47. Fleg JL, Stone GW, Fayad ZA, Granada JF, Hatsukami TS, Kolodgie FD, Ohayon J, Pettigrew R, Sabatine MS, Tearney GJ, Waxman S, Domanski MJ, Srinivas PR, Narula J. Detection of high-risk atherosclerotic plaque: report of the NHLBI Working Group on current status and future directions. *JACC Cardiovasc Imaging.* 2012;5(9):941-55.
48. Kerwin WS, Hatsukami T, Yuan C, Zhao XQ. MRI of carotid atherosclerosis. *AJR Am J Roentgenol.* 2013;200(3):W304-13.
49. Caravan P, Ellison JJ, McMurry TJ, Lauffer RB. Gadolinium(III) chelates as MRI contrast agents: Structure, dynamics, and applications. *Chem Rev.* 1999;99(9):2293-352.
50. Weissleder R, Hahn PF, Stark DD, Rummery E, Saini S, Wittenberg J, Ferrucci JT. Mr Imaging of Splenic Metastases - Ferrite-Enhanced Detection in Rats. *Am J Roentgenol.* 1987;149(4):723-6.
51. Weissleder R, Reimer P, Lee AS, Wittenberg J, Brady TJ. MR receptor imaging: ultrasmall iron oxide particles targeted to asialoglycoprotein receptors. *AJR Am J Roentgenol.* 1990;155(6):1161-7.
52. Lu AH, Salabas EL, Schuth F. Magnetic nanoparticles: synthesis, protection, functionalization, and application. *Angew Chem Int Ed Engl.* 2007;46(8):1222-44.
53. Reimer P, Weissleder R, Lee AS, Wittenberg J, Brady TJ. Receptor imaging: application to MR imaging of liver cancer. *Radiology.* 1990;177(3):729-34.
54. Ding Y, Hu Y, Jiang XQ, Zhang LY, Yang CZ. Polymer-monomer pairs as a reaction system for the synthesis of magnetic Fe₃O₄-polymer hybrid hollow nanospheres. *Angew Chem Int Edit.* 2004;43(46):6369-72.
55. Liu K, Wang MW, Lin WY, Phung DL, Grgis MD, Wu AM, Tomlinson JS, Shen CKF. Molecular Imaging Probe Development Using Microfluidics. *Curr Org Synth.* 2011;8(4):473-87.
56. McAtee MA, Choudhury RP. Targeted molecular imaging of vascular inflammation in cardiovascular disease using nano- and micro-sized agents. *Vascul Pharmacol.* 2013;58(1-2):31-8.
57. Lee SH, Kim BH, Na HB, Hyeon T. Paramagnetic inorganic nanoparticles as T1 MRI contrast agents. *Wiley Interdiscip Rev Nanomed Nanobiotechnol.* 2014;6(2):196-209.
58. Strijkers GJ, Mulder WJ, van Tilborg GA, Nicolay K. MRI contrast agents: current status and future perspectives. *Anticancer Agents Med Chem.* 2007;7(3):291-305.

59. Goel S, Miller A, Agarwal C, Zakin E, Acholonu M, Gidwani U, Sharma A, Kulbak G, Shani J, Chen O. Imaging Modalities to Identity Inflammation in an Atherosclerotic Plaque. *Radiol Res Pract.* 2015;2015:410967.
60. Zhang SH, Reddick RL, Piedrahita JA, Maeda N. Spontaneous hypercholesterolemia and arterial lesions in mice lacking apolipoprotein E. *Science.* 1992;258(5081):468-71.
61. Jawien J. The role of an experimental model of atherosclerosis: apoE-knockout mice in developing new drugs against atherogenesis. *Curr Pharm Biotechnol.* 2012;13(13):2435-9.
62. von Holt K, Lebrun S, Stinn W, Conroy L, Wallerath T, Schleef R. Progression of atherosclerosis in the Apo E-/ model: 12-month exposure to cigarette mainstream smoke combined with high-cholesterol/fat diet. *Atherosclerosis.* 2009;205(1):135-43.
63. Tamminen M, Mottino G, Qiao JH, Breslow JL, Frank JS. Ultrastructure of early lipid accumulation in ApoE-deficient mice. *Arterioscler Thromb Vasc Biol.* 1999;19(4):847-53.
64. De Leon H, Boue S, Schlage WK, Boukharov N, Westra JW, Gebel S, VanHooser A, Talikka M, Fields RB, Veljkovic E, Peck MJ, Mathis C, Hoang V, Poussin C, Deehan R, Stolle K, Hoeng J, Peitsch MC. A vascular biology network model focused on inflammatory processes to investigate atherogenesis and plaque instability. *J Transl Med.* 2014;12:185.
65. Plump AS, Smith JD, Hayek T, Aalto-Setala K, Walsh A, Verstuyft JG, Rubin EM, Breslow JL. Severe hypercholesterolemia and atherosclerosis in apolipoprotein E-deficient mice created by homologous recombination in ES cells. *Cell.* 1992;71(2):343-53.
66. Hopkins PN. Molecular biology of atherosclerosis. *Physiol Rev.* 2013;93(3):1317-542.
67. Smith JD, Breslow JL. The emergence of mouse models of atherosclerosis and their relevance to clinical research. *J Intern Med.* 1997;242(2):99-109.
68. Henke J, Baumgartner C, Roltgen I, Eberspacher E, Erhardt W. Anaesthesia with midazolam/meDETomidine/fentanyl in chinchillas (*Chinchilla lanigera*) compared to anaesthesia with xylazine/ketamine and meDETomidine/ketamine. *J Vet Med A Physiol Pathol Clin Med.* 2004;51(5):259-64.
69. Prince MR, Meaney JF. Expanding role of MR angiography in clinical practice. *Eur Radiol.* 2006;16 Suppl 2:B3-8.
70. Finn JP, Nguyen KL, Han F, Zhou Z, Salusky I, Ayad I, Hu P. Cardiovascular MRI with ferumoxytol. *Clin Radiol.* 2016;71(8):796-806.
71. Makowski MR, Preissel A, von Bary C, Warley A, Schachoff S, Keithan A, Cesati RR, Onthank DC, Schwaiger M, Robinson SP, Botnar RM. Three-dimensional imaging of the aortic vessel wall using an elastin-specific magnetic resonance contrast agent. *Invest Radiol.* 2012;47(7):438-44.
72. Botnar RM, Wiethoff AJ, Ebersberger U, Lacerda S, Blume U, Warley A, Jansen CH, Onthank DC, Cesati RR, Razavi R, Marber MS, Hamm B, Schaeffter T, Robinson SP, Makowski MR. In vivo assessment of aortic aneurysm wall integrity using elastin-specific molecular magnetic resonance imaging. *Circ Cardiovasc Imaging.* 2014;7(4):679-89.
73. Okamura H, Pisani LJ, Dalal AR, Emrich F, Dake BA, Arakawa M, Onthank DC, Cesati RR, Robinson SP, Milanesi M, Kotek G, Smit H, Connolly AJ, Adachi H, McConnell MV, Fischbein MP. Assessment of elastin deficit in a Marfan mouse aneurysm model using an elastin-specific magnetic resonance imaging contrast agent. *Circ Cardiovasc Imaging.* 2014;7(4):690-6.
74. Saba L, Saam T, Jager HR, Yuan C, Hatsukami TS, Saloner D, Wasserman BA, Bonati LH, Wintermark M. Imaging biomarkers of vulnerable carotid plaques for stroke risk prediction and their potential clinical implications. *Lancet Neurol.* 2019;18(6):559-72.

7. Publikationsliste

Erstautorenschaft

1. Reimann C, Brangsch J, Colletini F, Walter T, Hamm B, Botnar RM, Makowski MR. Molecular imaging of the extracellular matrix in the context of atherosclerosis. *Advanced drug delivery reviews*. 2017;113:49-60
2. Reimann C, Brangsch J, Kaufmann JO, Adams LC, Onthank DC, Robinson SP, Botnar RM, Collettini F, Makowski MR. Contrast-enhanced magnetic resonance angiography using a novel elastin-specific molecular probe in an experimental animal model. *Contrast media & molecular imaging*. 2018;2018:9217456
3. Reimann C, Brangsch J, Adams LC, Thöne-Reineke C, Hamm B, Makowski MR. Mr angiography of the head/neck vascular system in mice on a clinical mri system. *Contrast Media & Molecular Imaging*. 2019;2019:9
4. Reimann C, Brangsch J, Kaufmann JO, Adams LC, Onthank DC, Thone-Reineke C, Robinson SP, Hamm B, Botnar RM, Makowski MR. Dual-probe molecular MRI for the in vivo characterization of atherosclerosis in a mouse model: Simultaneous assessment of plaque inflammation and extracellular-matrix remodeling. *Scientific reports*. 2019;9(1):13827

Co-Autorenschaft

5. Schreiter V, Reimann C, Geisel D, Schreiter NF. Nuclear medicine imaging of prostate cancer. *RoFo : Fortschritte auf dem Gebiete der Rontgenstrahlen und der Nuklearmedizin*. 2016;188:1037-1044
6. Brangsch J, Reimann C, Collettini F, Buchert R, Botnar RM, Makowski MR. Molecular imaging of abdominal aortic aneurysms. *Trends in molecular medicine*. 2017;23:150-164
7. Jansen CHP, Reimann C, Brangsch J, Botnar RM, Makowski MR. In vivo mr-angiography for the assessment of aortic aneurysms in an experimental mouse model on a clinical mri scanner: Comparison with high-frequency ultrasound and histology. *PloS one*. 2017;12:e0178682
8. Jansen CHP, Brangsch J, Reimann C, Adams L, Hamm B, Botnar RM, Makowski MR. In vivo high-frequency ultrasound for the characterization of thrombi associated with aortic aneurysms in an experimental mouse model. *Ultrasound in medicine & biology*. 2017;43:2882-2890
9. Botnar RM, Brangsch J, Reimann C, Janssen CHP, Razavi R, Hamm B, Makowski MR. In vivo molecular characterization of abdominal aortic aneurysms using fibrin-specific magnetic resonance imaging. *Journal of the American Heart Association*. 2018;7
10. Brangsch J, Reimann C, Kaufmann JO, Adams LC, Onthank DC, Thone-Reineke C, Robinson SP, Buchholz R, Karst U, Botnar RM, Hamm B, Makowski MR. Concurrent molecular magnetic resonance imaging of inflammatory activity and extracellular matrix degradation for the prediction of aneurysm rupture. *Circ Cardiovasc Imaging*. 2019;12:e008707
11. Keller S, Chapiro J, Brangsch J, Reimann C, Collettini F, Sack I, Savic LJ, Hamm B, Goldberg SN, Makowski M. Quantitative MRI for Assessment of Treatment Outcomes in a Rabbit VX2 Hepatic Tumor Model. *J Magn Reson Imaging*. 2019.
12. Adams LC, Bressem KK, Brangsch J, Reimann C, Nowak KJ, Brenner W, Makowski MR. Quantitative 3D Assessment of ^{68}Ga -DOTATOC PET/MRI with Diffusion-Weighted Imaging to Assess Imaging Markers for Gastroenteropancreatic Neuroendocrine Tumors: Preliminary Results. *J Nucl Med*. 2020;61(7):1021-1027.

13. Adams LC, Brangsch J, Reimann C, Kaufmann JO, Nowak K, Buchholz R, Karst U, Botnar RM, Hamm B, Makowski MR. Noninvasive imaging of vascular permeability to predict the risk of rupture in abdominal aortic aneurysms using an albumin-binding probe. *Sci Rep.* 2020;10(1):3231.
14. Adams LC, Brangsch J, Reimann C, et al. Simultaneous molecular MRI of extracellular matrix collagen and inflammatory activity to predict abdominal aortic aneurysm rupture. *Sci Rep.* 2020;10(1):15206. Published 2020 Sep 16. doi:10.1038/s41598-020-71817-x
15. Keller S, Borde T, Brangsch J, et al. Native T1 Mapping Magnetic Resonance Imaging as a Quantitative Biomarker for Characterization of the Extracellular Matrix in a Rabbit Hepatic Cancer Model. *Biomedicines.* 2020;8(10):412. Published 2020 Oct 13. doi:10.3390/biomedicines8100412
16. Keller S, Borde T, Brangsch J, et al. Assessment of the hepatic tumor extracellular matrix using elastin-specific molecular magnetic resonance imaging in an experimental rabbit cancer model. *Sci Rep.* 2020;10(1):20785. Published 2020 Nov 27. doi:10.1038/s41598-020-77624-8
17. Brangsch J, Reimann C, Kaufmann JO, et al. Molecular MR-Imaging for Noninvasive Quantification of the Anti-Inflammatory Effect of Targeting Interleukin-1 β in a Mouse Model of Aortic Aneurysm. *Mol Imaging.* 2020;19:1536012120961875. doi:10.1177/1536012120961875
18. Collettini F, Reimann C, Brangsch J, et al. Elastin-specific MRI of extracellular matrix-remodelling following hepatic radiofrequency-ablation in a VX2 liver tumor model. *Sci Rep.* 2021;11(1):6814. Published 2021 Mar 25. doi:10.1038/s41598-021-86417-6

8. Danksagung

Zu allererst möchte ich mich bei meinem Doktorvater Prof. Dr. med. Marcus Richard Makowski für die herausragende Betreuung meiner Dissertation bedanken. In allen Stadien meiner Doktorarbeit unterstützte er mich mit seiner Erfahrung. Am Ende dieser Zusammenarbeit stehen mehrere veröffentlichte Erstautorenschaften sowie mehrere Co-Autorenschaften.

Des Weiteren möchte ich mich besonders bei meiner Doktormutter Prof. Dr. med. vet. Christa Thöne-Reineke für die herzliche und äußerst freundliche Betreuung und Unterstützung bedanken. Insbesondere für die große Hilfsbereitschaft und organisatorische Hilfestellung bei dieser translationalen Doktorarbeit möchte ich danken.

Ein ganz besonderes Dankeschön geht an die Mitarbeiter/innen der AG Makowski. Es ist schön auf ein so breit aufgestelltes Team zurückgreifen zu können. Die gesamte Erfahrung im Zusammenhang mit meiner Arbeit in der Klinik für Radiologie wird mir zeitlebens positiv im Gedächtnis verbleiben.

Schlussendlich möchte ich mich bei meinen Eltern, die mir meinen bisherigen Lebensweg ermöglichten, von ganzem Herzen für ihre uneingeschränkte Unterstützung bedanken. Ihnen widme ich diese Arbeit.

9. Selbstständigkeitserklärung

„Ich, Carolin Reimann, versichere an Eides statt, dass ich die vorgelegte Dissertation mit dem Thema: „Entwicklung und Evaluierung neuer niedrig-molekularer Sonden für die Charakterisierung von Gefäßerkrankungen mittels der Magnetresonanztomographie (MRT)“ selbstständig und ohne nicht offengelegte Hilfe Dritter verfasst und keine anderen als die angegebenen Quellen und Hilfsmittel genutzt habe.

Alle Stellen, die wörtlich oder dem Sinne nach auf Publikationen oder Vorträgen anderer Autoren beruhen, sind als solche in korrekter Zitierung (siehe „Uniform Requirements for Manuscripts (URM)“ des ICMJE -www.icmje.org) kenntlich gemacht.

Sämtliche Publikationen, die aus dieser Dissertation hervorgegangen sind und bei denen ich Autor bin, entsprechen den URM (s.o) und werden von mir verantwortet.

Die Bedeutung dieser eidestattlichen Versicherung und die strafrechtlichen Folgen einer unwahren eidestattlichen Versicherung (§156,161 des Strafgesetzbuches) sind mir bekannt und bewusst.“

Berlin, 28.07.2020

Carolin Reimann



mbvberlin mensch und buch verlag

49,90 Euro | ISBN: 978-3-96729-114-8